DOI:
10.1016/j.jaci.2022.04.027

Single-cell analysis implicates Th17 to Th2 plasticity in the pathogenesis of palmoplantar pustulosis (PPP)

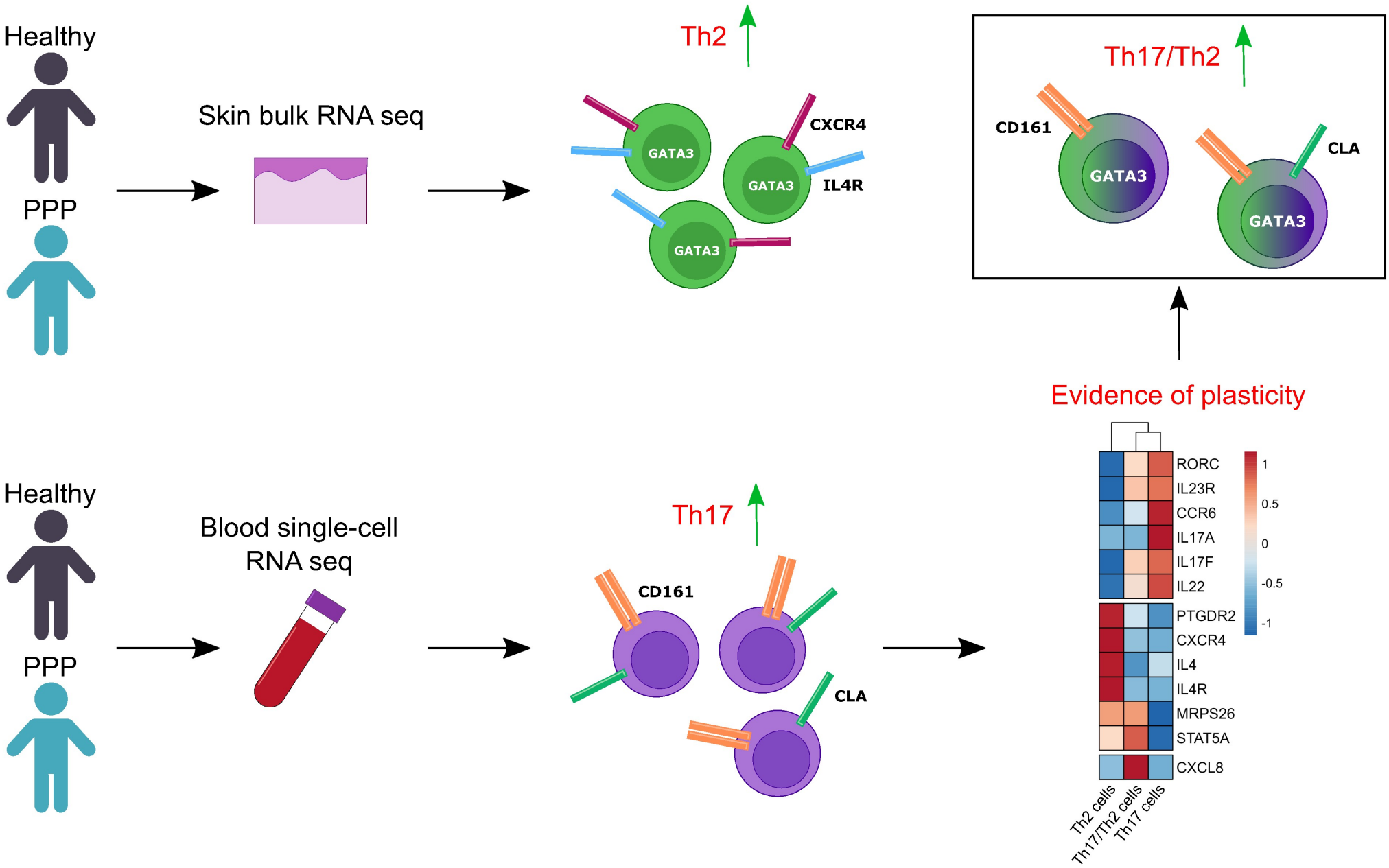

Single-cell analysis implicates Th17 to Th2 cell plasticity in the pathogenesis of palmoplantar pustulosis

Daniel McCluskey[1], Natashia Benzian-Olsson[1], Satveer K Mahil[2], Nina Karoliina Hassi[1], Christian T Wohnhaas[3], The APRICOT and PLUM study team, A David Burden[4], Christopher EM Griffiths[5], John R Ingram[6], Nick J Levell[7], Richard Parslew[8], Andrew E Pink[2], Nick J Reynolds[9], Richard B Warren[5], Sudha Visvanathan[10], Patrick Baum[3], Jonathan N Barker[2], Catherine H Smith[2], Francesca Capon[1,*]

[1]Department of Medical and Molecular Genetics, Faculty of Life Sciences and Medicine, King's College London, London, UK

[2]St John's Institute of Dermatology, Faculty of Life Sciences and Medicine, King's College London, London, UK

[3]Boehringer Ingelheim Pharma GmbH & Co. KG, Biberach, Germany

[4]Institute of Infection Immunity and Inflammation, University of Glasgow, Glasgow, UK

[5]Dermatology Centre, Salford Royal NHS Foundation Trust, NIHR Manchester Biomedical Research Centre, University of Manchester, Manchester, UK

[6]Department of Dermatology, Division of Infection & Immunity, Cardiff University, Cardiff, UK

[7]Norwich Medical School, University of East Anglia, Norwich, UK

[8]Department of Dermatology, Royal Liverpool Hospitals, Liverpool, UK

[9]Translational and Clinical Research Institute, Newcastle University and Department of Dermatology and NIHR Newcastle Biomedical Research Centre, Newcastle Hospitals NHS Foundation Trust, Newcastle upon Tyne, UK

[10]Boehringer Ingelheim Pharmaceuticals, Ridgefield, USA.

*Correspondence to: Francesca Capon, 9th floor Tower Wing, Guy's Hospital, London SE1 9RT, UK. Phone: +44 207 188 8079; Email: francesca.capon@kcl.ac.uk

Funding

We acknowledge support from the Department of Health via the National Institute for Health Research (NIHR) BioResource Clinical Research Facility and comprehensive Biomedical Research Centre awards to Guy's and St Thomas' NHS Foundation Trust in partnership with King's College London and King's College Hospital NHS Foundation Trust (guysbrc-2012-1).

We also acknowledge support from the Newcastle NIHR Biomedical Research Centre.

The APRICOT trial was funded by the Efficacy and Mechanism Evaluation (EME) Programme, a UK Medical Research Council (MRC) and NIHR partnership (grant EME 13/50/17 to CHS, FC, JNB, ADB, RBW, NJR and CEMG). This work was supported by the European Academy of Dermatology and Venereology (grant PPRC-2018-25 to FC and JNB) and the Psoriasis Association (Grant BSTOP50/5 to CHS). DMc is supported by the MRC (grant MR/R015643/1) and King's College London as member of the MRC Doctoral Training Partnership in Biomedical Sciences. NBO was funded by a NIHR pre-doctoral fellowship (grant NIHR300473).

SKM is funded by an MRC Clinical Academic Research Partnership award (MR/T02383X/1).

CEMG is funded in part by the NIHR Manchester Biomedical Research Centre and is an NIHR Emeritus Senior Investigator. NJR is a NIHR Senior Investigator. He acknowledges support from the Newcastle MRC/EPSRC Molecular Pathology Node and the Newcastle NIHR Medtech and In vitro diagnostic Co-operative. RBW is supported by the Manchester NIHR Biomedical Research Centre. The views expressed in this publication are those of the authors and not necessarily those of the MRC, NHS, NIHR or the Department of Health.

Conflicts of interests

FC and JNB have received funding from Boehringer-Ingelheim. CTW, PB and SV are Boehringer-Ingelheim employees. JRI is Editor-in-Chief of the British Journal of Dermatology and receives an author honorarium from UpToDate. He is a Consultant for UCB Pharma, Novartis, Boehringer Ingelheim and ChemoCentryx and participated in Advisory Boards for Kymera Therapeutics and Viela Bio, all in the field of hidradenitis suppurativa. He is a co-copyright holder of the HiSQOL and Patient Global Assessment instruments for hidradenitis suppurativa. RBW has received research grant and/or consultancy fees from AbbVie, Almirall, Amgen, Arena, Astellas, Avillion, Biogen, Boehringer Ingelheim, Bristol Myers Squibb, Celgene, DiCE, GSK, Janssen, Lilly, Leo, Medac, Novartis, Pfizer, Sanofi, Sun Pharma, UCB and UNION.

Abstract

Background: Palmoplantar pustulosis (PPP) is a severe inflammatory skin disorder, characterised by eruptions of painful, neutrophil-filled pustules on the palms and soles. While PPP has a profound effect on quality of life, it remains poorly understood and notoriously difficult to treat.

Objective: We sought to investigate the immune pathways that underlie the pathogenesis of PPP.

Methods: We applied bulk- and single-cell RNA-sequencing methods to the analysis of skin biopsies and peripheral blood mononuclear cells. We validated our results by flow cytometry and immune fluorescence microscopy

Results: Bulk RNA-sequencing of patient skin detected an unexpected signature of T-cell activation, with a significant overexpression of several Th2 genes typically upregulated in atopic dermatitis. To further explore these findings, we carried out single-cell RNA-sequencing in peripheral blood mononuclear cells of healthy and affected individuals. We found that the memory CD4+T-cells of PPP patients were skewed towards a Th17 phenotype, a phenomenon that was particularly significant among CLA+ skin-homing cells. We also identified a subset of memory CD4+ T-cells which expressed both Th17 (*KLRB1/*CD161) and Th2 (*GATA3*) markers, with pseudo-time analysis suggesting that the population was the result of Th17 to Th2 plasticity. Interestingly, the GATA3+/CD161+ cells were over-represented among the PBMCs of affected individuals, both in the scRNA-seq dataset and in independent flow-cytometry experiments. Dual positive cells were also detected in patient skin by means of immune fluorescence microscopy.

Conclusions: These observations demonstrate that PPP is associated with complex T-cell activation patterns and may explain why biologics that target individual T-helper populations have shown limited therapeutic efficacy.

Clinical implications: The simultaneous activation of Th17 and Th2 responses in PPP supports the therapeutic use of agents that inhibit multiple T-cell pathways.

Capsule summary: Transcription profiling of PPP patients reveals that Th2 responses are dominant in skin, while Th17 activation is prominent in the circulation. Substantial Th17 to Th2 plasticity was detected in both compartments.

Key words: Single-cell RNA-sequencing, scRNA-seq, T-cell plasticity, palmoplantar pustulosis, PPP,

Abbreviations: NL, non-lesional; PBMCs, peripheral blood mononuclear cells; PPP, palmoplantar pustulosis, scRNA-seq, single-cell RNA-sequencing

INTRODUCTION

Palmoplantar pustulosis (PPP) is a chronic and debilitating skin disorder, which manifests with the eruption of neutrophil-filled pustules on the palms and the soles. These painful lesions typically occur on a background of inflamed skin, causing functional and occupational disability [1].

While PPP has a profound impact on quality of life, its causes remain poorly understood. The disease preferentially affects adult females and is associated with cigarette smoking [2]. However, the mechanisms mediating the effects of sex and tobacco exposure are unclear [3]. Although it has been suggested that PPP shares common genetic determinants with other pustular diseases, *IL36RN* mutations (which are frequently observed in generalised pustular psoriasis) have only been reported in a small number of cases[2, 4].

Owing to this limited understanding of disease pathogenesis, evidence-based guidelines for the management of PPP are lacking[5]. The response to conventional systemic therapeutics (oral retinoids, methotrexate and cyclosporine) is variable and their prolonged use can have toxic effects[5]. Clinical trials of IL-1 (anakinra) and IL-36 (spesolimab) blockers have been carried out on the assumption that PPP has an autoinflammatory pathogenesis, but the studies undertaken so far could not provide evidence of broad clinical efficacy[6, 7]. IL-17 (secukinumab) and IL-23 (guselkumab) inhibitors have also been assessed. While these biologics reduced disease severity, skin clearance was achieved in <30% of patients[8, 9].

Here, we sought to identify disease drivers and potential therapeutic targets for PPP, through the transcription profiling of patients' cells. We uncovered a complex immunological landscape, where Th2 cell activation dominates in skin while circulating T-cells are skewed towards a Th17 phenotype. We also observed evidence of increased Th17 to Th2 plasticity in the circulating and skin homing T-lymphocytes of affected individuals. These findings point to the activation of diverse T-helper populations in PPP and warrant the investigation of small molecule therapeutics that can inhibit multiple signaling pathways.

METHODS

Study participants

This work was carried out in accordance with the principles of the declaration of Helsinki and with written informed consent of all participants. PPP was diagnosed based on clinical examination and the consensus criteria set by the European Rare And Severe Psoriasis Expert Network

(ERASPEN)[10]. Affected individuals were ascertained through the APRICOT clinical trial (approved by the London Dulwich Research Ethics Committee; ref: 16/LO/0436) or its sister research study PLUM (approved by the London Bridge Research Ethics Committee; ref: 16/LO/2190). Age- and sex- matched healthy volunteers were also recruited to the PLUM study. Clinical and demographic features of study participants are summarised in Table E1.

Sampling and RNA-sequencing of skin biopsies

Two-millimetre acral skin biopsies were obtained from healthy controls or APRICOT trial participants. Patients were recruited at their baseline visit, following recommended washout period and before treatment initiation[6]. Lesional biopsies were taken from inflamed skin (avoiding pustules), while non-lesional biopsies were sampled from adjacent, uninvolved skin. Total RNA was extracted using a miRVana isolation kit (ThermoFisher Scientific). Following poly-A selection and library preparation, samples were run on an Illumina HiSeq instrument to generate 150bp paired-end reads.

scRNA-seq

Peripheral Blood Mononuclear Cells (PBMCs) were re-suspended in fetal calf serum (FCS, Invitrogen)/10% DMSO and stored in liquid nitrogen for up to 4 weeks. On the day of the experiment, cells were thawed, counted and loaded on a Chromium Single Cell 3' Chip (10x Genomics), as described elsewhere [11]. Libraries were prepared using the Single Cell 3' Reagent Kits v3 (10x Genomics) and sequenced on a HiSeq4000 instrument (Illumina).

scRNA-seq data analysis

Sequence reads were processed, aligned to the GRCh38 reference genome and annotated to Ensembl (release 86) genes, using Cell Ranger version 3.0.2 (10x Genomics). The healthy donor datasets published by Zheng et al[12] (n=3) and Schafflick et al[13] (n=5) were retrieved from the 10x Genomics portal (https://support.10xgenomics.com/single-cell-gene-expression/datasets) and the GEO repository (identifier GSE138266), respectively. The three datasets were then merged using Harmony[14] to correct for batch effects. The resulting gene expression matrix was processed with Seurat v3.0[15]. Quality control filters were first applied to remove cells with low (<300) or excessive (>5,000) numbers of detected genes. Cells where the percentage of mitochondrial gene reads

exceeded 20% were also excluded. Following log-normalisation and scaling of the data, variation due to the following sources was regressed out: sequencing batch, data origin (generated in-house, published by Zheng et al, published by Schafflick et al), smoking status, treatment with biologics and Unique Molecular Identifier (UMI).

After principal component analysis and construction of a K-nearest neighbour graph, unsupervised clustering was undertaken with a resolution of 0.4. The resulting cell clusters were visualised by UMAP. Cluster markers were computed with the FindAllMarkers Seurat function and cell identities were annotated based on the expression of canonical marker genes. SingleR[16] was used to validate cell identities and to annotate the phenotypes of memory CD4+ T cells as Th1, Th2 or Th17. The full resource published by Monaco et al[17] was used as a reference dataset.

For the pseudotime analysis, the three CD4+ T-cell clusters (naïve CD4+, memory CD4+ T1 and memory CD4+T2) were manually retrieved and processed with Slingshot v. 1.7.0[18]. Following UMAP dimensionality reduction with the uwot package, a minimum spanning tree was fitted to the clusters. The resulting trajectory was smoothed by iteratively fitting principal curves.

Statistics

Cell abundance and gene expression levels were compared in cases vs controls, using the Mann-Whitney test. The significance of overlaps observed in Venn diagrams was computed with Fisher's exact test. All tests were implemented in R v4.02. P-values <0.05 were deemed statistically significant.

RESULTS

A prominent Th2 signature in PPP non-lesional skin

To explore the immune pathways that are disrupted in PPP, we first carried out bulk RNA-sequencing in three paired, lesional and non-lesional skin biopsies, obtained from the palmar or plantar (acral) skin of affected individuals (Table E1). We identified a total of 1,050 differentially expressed genes (log2[Fold-change] >|0.5|; False Discovery Rate (FDR) <0.05) (Figure E1a, Table E2a). In keeping with the neutrophilic nature of PPP lesions, these showed a significant enrichment for innate pathways (e.g., *Granulocyte adhesion and diapedesis* and *IL-8 signaling;* FDR<10^{-3} for both), (Figure E1a).

We obtained similar results when we compared the three lesional samples with healthy acral skin donated by seven volunteers, matched for age, sex and smoking status (Table E1). In fact, we identified 1,323 differentially expressed genes showing a very marked enrichment for innate pathways (e.g., *Granulocyte adhesion and diapedesis*, FDR<10^{-8}). At the same time, we also uncovered an unexpected over-representation of T cell related genes (e.g., *T cell receptor signaling*, FDR<10^{-6}) (Figure E1b).

To further explore these findings while avoiding the confounding effects of end-stage inflammation (i.e. the secondary upregulation of genes that do not contribute to disease pathogenesis), we next compared non-lesional (NL) PPP biopsies (n=8) with healthy skin (n=7). We observed 531 differentially expressed genes (Figure 1a; Figure E1c; Table E2b). In keeping with the results of genetic studies and clinical trials[2, 6], we found limited evidence for a sustained upregulation of IL-36 signaling. While *IL36A* (encoding IL-36α) was overexpressed in NL compared to control skin, the mRNA levels of *IL36B*, *IL36G* and *IL1RL2* (respectively encoding IL-36β, IL-36γ and IL-36R) were comparable in the two groups.

A closer inspection of the 531 genes that were differentially expressed in NL PPP skin revealed a pervasive enrichment of T-cell activation pathways (e.g., *CD28 signaling in T-helper cells* and *ICOS-ICOSL signaling in T-helper cells*; FDR<10^{-8} for both), with significant evidence for an involvement of Th2 (FDR=$1.2\text{x}10^{-8}$) and to a lesser extent, Th1 (FDR=$5.6\text{x}10^{-7}$) responses (Figure 1b, Table E3a). Conversely, the enrichment of Th17-related genes was limited (FDR=0.001) (Table E3a). In keeping with these observations, an upstream regulator analysis demonstrated a significant over-representation of genes induced by IFN-γ, IL-4 (FDR<10^{-15} for both) and IL-13 (FDR<10^{-10}) (Figure 1c). This was accompanied by a modest enrichment of IL-17 dependent loci (FDR<10^{-3}) (Table E3b).

To further explore the significance of these findings, we re-analysed publicly available skin RNA-sequencing data, including patients with Th2- (atopic dermatitis, n=27) and Th17- (plaque psoriasis, n=28) mediated conditions, as well as healthy volunteers (n=38)[19]. We identified 510 genes that were differentially expressed in NL atopic dermatitis skin compared to site-matched control biopsies (log2[Fold-change] >|0.5|; False Discovery Rate (FDR) <0.05). When we compared these genes with the 531 that were differentially expressed in NL PPP skin, we observed a very significant overlap between the two datasets (111 shared genes; odds ratio over genomic background: 18.8). While this observation further confirmed the upregulation of Th2 pathways in

PPP skin, the evidence for Th17 activation was less significant. In fact, there was a limited overlap between the NL PPP dataset and the 630 genes that were differentially expressed in NL psoriasis skin compared to control (53 shared genes, odds ratio: 5.4) (Figure 1d).

To further validate these findings, we used real-time PCR to analyse uninvolved acral skin obtained from 8 PPP cases and 7 healthy controls (including 5 cases and 3 controls who had not been included in the RNA-sequencing experiment). This confirmed that key Th2 genes such as *IL4R*, *CCL13*/MCP-4 (which activates the CCR3 receptor expressed by Th2 cells[20]) and *CXCR4* (which is expressed on the surface of Th2 cells and eosinophils[21]) were upregulated in NL PPP skin. A moderate increase of Th1 (*CXCR3*) and Th17 markers (*IL17A*) was also observed (Figure 1e).

Taken together, these observations identify a marked signature of Th2 activation in NL PPP skin, with evidence for a more modest involvement of Th17 pathways.

Increased abundance of two circulating T-cell subsets in PPP

We next investigated whether systemic immune responses were also deregulated in PPP. We therefore carried out single-cell RNA-sequencing (scRNA-seq) in PBMCs obtained from 7 PPP cases and 4 age- and gender-matched healthy volunteers (Table E1). Following capture on a 10x Genomics platform, 3'-end sequencing and quality control, we observed 58,412 viable cells (Table E4). To maximise statistical power, we expanded this dataset by including eight publicly available control samples, which had been processed on the same platform used in our experiment, yielding comparable cell numbers[12, 13] (Figure E2a). To integrate these external healthy controls in our resource, we undertook batch correction with the Harmony algorithm[14], obtaining a total of 93,262 cells (Figure 2a and Figure E2b).

When we analysed the merged dataset with Seurat[15], we identified 13 cell clusters, which we visualised by uniform manifold approximation and projection (UMAP) (Figure 2a and Figure E2c). The annotation of cell identities (implemented by manual inspection of canonical marker genes (Table E5) and validated with SingleR [16]) revealed that the clusters corresponded to natural killer cells, monocytes (CD14+ and CD16+ subsets), myeloid and plasmacytoid dendritic cells, B-cells (memory and naïve subsets) and T-cells (two naïve, one effector and three memory subsets) (Figure 2a-c, Figure E3a). While unconventional T lymphocytes (Mucosal-Associated Invariant T cells and γδ T-cells) were also detected, they did not form separate clusters (Figure E3b-c).

A comparison of cases and controls showed that innate cells (monocytes, natural killer and dendritic cells) were found at similar frequencies in the two groups. Conversely, two of the T-cell subsets were more abundant among affected individuals. These corresponded to clusters that we had initially labelled as memory CD4+ T1 (accounting for 27.9% cells in cases vs 23.1% in controls; P=0.02) and memory CD4+ T2 (3.6% cells in cases vs 1.8% in controls; $P<10^{-4}$) cells (Figure 2d-e). Of note, control cell frequencies were comparable between the samples recruited in house and those retrieved from public databases, showing that the analysis was not skewed by the inclusion of external datasets (Figure E2d).

To further investigate the identity of the two CD4+ memory populations, we assessed whether they expressed Cutaneous-Lymphocyte-Associated antigen (CLA), a well-known skin homing marker. We found that cells expressing *SELPLG* (the gene encoding CLA) were a minority among memory CD4+ T1 lymphocytes, but very frequent in the CD4+ T2 subset (28.0% vs. 51.2% P<0.0001). Of note, *ITGB7* (encoding the gut-homing receptor integrin beta seven) was virtually undetectable in the latter population, confirming the specificity of the skin-homing phenotype.

Interestingly, CD4+ T2 cells also expressed *ITGAE*, which encodes the CD103 antigen (Figure 2f). This identifies tissue-resident memory T-cells (T_{RM} cells) that have re-entered the circulation and are migrating to secondary skin sites[22]. Thus, the memory CD4+ T1 and CD4+ T2 clusters correspond to circulating and skin-homing populations, respectively.

Th17 skewing in the CD4+ memory T-cells of affected individuals.

We next investigated the phenotype of CD4+ memory T-cells in affected individuals. Like other authors[23, 24], we found that it was not possible to separate the different T-helper subsets into specific subclusters. We therefore used SingleR to annotate Th1, Th2 and Th17 cell identities within the existing CD4+ T1 and CD4+ T2 clusters. This revealed a significant enrichment of Th17 lymphocytes among the memory CD4+ T-cells of PPP cases. The effect was observed in both the circulating (CD4+ T1) and the skin homing (CD4+ T2) population, but was especially marked in the latter, where the median Th17 fraction was 13.9% in cases vs 0.5% in controls ($P<10^{-4}$) (Figure 3a and E4a). No further abnormalities were consistently observed in both memory CD4+ compartments (Figure 3a, Figure E4a).

To validate these findings with another methodology, we examined the Th1, Th2 and Th17 transcriptional signatures developed by Cano-Gamez et al.[23]. This confirmed that Th17 gene

expression was elevated in both circulating and skin-homing cells of affected individuals, while Th1 and Th2 scores were not (Figure E4b). In keeping with these observations, an analysis of the transcription factors driving Th1 (*TBX21*/T-bet), Th2 (*GATA3*) and Th17 (*RORG*/RORγt) lineage commitment, demonstrated that *RORG* (but not *TBX21* or *GATA3*) was upregulated in the memory CD4+T cells of PPP patients (Figure 3b). Of note, the over-expression of *RORG* was not replicated in memory CD8+ T cells (Figure E4c), which argues against a pathogenic involvement of Tc1 7 lymphocytes.

Taken together, these observations demonstrate a dominant Th17 phenotype in the circulating memory CD4+ T-cells of individuals affected by PPP.

Increased Th17 to Th2 plasticity in the CD4+ memory T-cells of affected individuals

Given the different T-cell responses observed in PPP skin (Th2 activation) and blood (Th17 skewing), we investigated the possibility that T-helper cell plasticity may contribute to disease pathogenesis.

It is now well established that changes in the cytokine environment can modulate the identity of Th17 cells and induce a shift towards Th1 or Th2 phenotypes[25, 26]. We therefore sought to determine the extent of Th17 cell plasticity, in PPP cases and healthy controls.

We first queried the scRNA-seq data generated in circulating and skin-homing, CD4+ memory T-lymphocytes. Specifically, we searched for cells that expressed both *GATA3* and *KLRB1*/CD161, which we selected as readily detectable Th2 and Th17 markers. This identified a subset of CD4+ memory T-cells that expressed both genes. Unsupervised hierarchical clustering showed that the GATA3+/CD161+ cells were more closely related to Th17 than Th2 lymphocytes (Figure 4a), as the expression of *RORG* and *IL23R* was readily detectable in dual-positive cells, while *IL4R* transcript levels were low (Figure 4b, Figure E5a).

While the simultaneous presence of GATA3 and CD161 has been documented in Th2A cells (a Th2 subtype associated with allergic disease[27]), our dual positive population did not show well-established Th2A markers such as *PPARG*, *PTGS2* or *HPGDS* [27] (Figure 4b, Figure E5b). Th9 signature genes such as *SPI1/*PU.1 and *BATF*[28] were likewise weakly expressed (Figure 4b, Figure E5b). Conversely, the GATA3+/CD161+ cells in our dataset had the same *CCR6+/RORG+/GATA3+/CXCL8+* phenotype as a Th17/Th2 subset observed among asthmatic patients[29, 30]. Interestingly, Cosmi et al showed that these Th17/Th2 cells can be derived from Th17

(CCR6+/CD161+) lymphocytes in the presence of IL-4 and that they can acquire functional Th2 characteristics (despite low *IL4R* expression), alongside their Th17 phenotype[29].

Here, we further explored the correlation between GATA3+/CD161+, Th17 and Th2 cells, by carrying out a pseudotime analysis of the entire CD4+ T-cell compartment. Using Slingshot [18], we found that GATA3+/CD161+ cells appeared later in pseudotime compared to both Th17 and Th2 cells (Figure 4c). Of note, the expression of *GATA3* and *KLRB1*/CD161 continued to rise steadily during pseudotime, reflecting the pattern observed for Th17 genes such as *RORC* and *IL23R*. Conversely, the levels of Th2 markers such as *CXCR4* and *PTGDR2* peaked and then fell sharply (Figure 4d). This is in keeping with the notion that the dual positive cells differentiate from Th17 rather than Th2 lymphocytes.

We next investigated the pathogenic significance of the CD161+/GATA3+ population. We observed that the dual positive cells were more abundant among the memory CD4+ T cells of PPP cases compared to those of healthy controls (13.7% vs 6.3%, P=0.004) (Figure 4e).

This difference was consistently observed among circulating (CD4+ T1) and skin-homing (CD4+ T2) T lymphocytes (Figure E5c).

Thus, we have identified a Th17/Th2 population that is associated with PPP.

Experimental validation of increased Th17 and Th17/Th2 cell abundance in PPP cases

We next sought to validate the scRNA-seq findings through the flow-cytometry analysis of PBMCs obtained from 6 affected individuals and 6 healthy volunteers (including 4 cases and 4 controls that had not been included in the scRNA-seq experiment). We found that the overall abundance of memory CD4+ T cells and Th17 cells was comparable in cases and controls (Figure E6a and E6b). However, the frequency of Th17 cells among skin-homing T-lymphocytes was elevated in individuals with PPP (9.8% vs 5.2% in healthy volunteers; P=0.03) (Figure 5a), reflecting the pattern observed by scRNA-seq. Likewise, Th17/Th2 cells were more abundant in affected compared to unaffected subjects. This effect was observed in the overall memory CD4+ T cell compartment (9.1% vs 6.6%, P=0.009) and also documented in the skin-homing population (6.1% vs. 4.3% P=0.04). (Figure 5b and 5c; Figure E6c).

To further examine the pathogenic role of dual-positive cells, we carried out fluorescence microscopy in non-lesional PPP skin. We observed T-cell infiltration in the upper dermis, where GATA3+/CD161+ cells were clearly visible (Figure 6, Figure E7).

Thus, dual positive Th17/Th2 cells are over-represented among the skin homing CD4+ T cells of affected individuals and readily detectable in their dermal infiltrates.

DISCUSSION

The purpose of this study was to achieve a better understanding of the immunological determinants of PPP, a condition that remains poorly understood at the aetiological level and recalcitrant to treatment in real-world practice [1].

We applied hypothesis-free transcriptomic approaches to a tightly phenotyped PPP resource that met the rigorous inclusion criteria of the APRICOT clinical trial [6]. We focused on cells (circulating PBMCs) and tissues (non-lesional skin) that were not affected by overt inflammation, so that we could survey the immune landscape of the disease in an unbiased fashion. The advantages of this approach are exemplified by the results of the initial RNA-sequencing experiment, where the comparison of lesional vs non-lesional biopsies detected a predictable upregulation of innate pathways in involved skin. Conversely, the analysis of non-lesional vs control samples revealed an unexpected and very prominent signature of T cell activation, in uninvolved patient skin. The evidence for the activation of Th2 lymphocytes was particularly significant, whereas the enrichment of Th17 related pathways was relatively modest. This argues against the traditional classification of PPP as a clinical variant of plaque psoriasis [1] and highlights hitherto unsuspected similarities with atopic dermatitis.

The pathogenic involvement of T-cells was also supported by the results obtained in circulating PBMCs. As the use of Boolean flow-cytometry gates cannot fully recapitulate the immune populations derived by scRNA-seq cell clustering, there were some discrepancies between the results obtained with the two platforms. For example, scRNA-seq experiments showed an increased frequency of the memory CD4+ T1 and memory CD4+ T2 clusters among affected individuals. While the same trend was observed for the memory CD4+T cells detected by flow-cytometry, the difference between cases and controls was not statistically significant.

Importantly, our key findings were validated in both platforms. Thus, scRNA-seq and flow-cytometry experiments consistently showed a skewed Th17 phenotype for patient skin-homing T-lymphocytes. They also demonstrated an increased abundance of Th17/Th2 (GATA3+/CD161+) cells among PPP cases.

To the best of our knowledge, these results provide the first evidence of systemic abnormalities in PPP. They may also explain the common occurrence of extra-cutaneous, T-cell mediated co-morbidities (e.g., psoriatic arthritis, autoimmune thyroid disease) among affected individuals [3].

Our observation of increased Th17/Th2 cell abundance in PPP cases also suggests a pathogenic role for Th17 plasticity. Interestingly, Th17/Th2 cells have been detected in the blood and bronchoalveolar lavage of asthmatic individuals, where they have been characterised as IL-4/IL-17 producing cells [29, 30]. A similar enrichment in patient populations has been reported for IL-17/IFNγ producing cells (Th17/Th1) in rheumatoid arthritis. Thus, Th17 cells shifted towards Th1 or Th2 phenotypes are considered more pathogenic than their unshifted counterparts [25, 31]. Intriguingly, Th17 cell plasticity has also been associated with cigarette smoking [32], one of the main risk factors for PPP [2]. Thus, several lines of evidence support the notion that the Th17/Th2 cells detected in the blood and skin of PPP patients contribute to disease processes.

It has been hypothesised that Th17/Th2 and Th17/Th1 cells originate in complex inflammatory milieus that cannot be easily recapitulated by *in vitro* polarization protocols [25, 26]. This is in keeping with the multifaceted immune landscape we detected in PPP skin. While the limitations of bulk RNA-sequencing prevented us from dissecting these circuits, our analysis uncovered a clear upregulation of distinct cytokine networks.

The simultaneous activation of multiple immune pathways in PPP skin would also explain the limited therapeutic efficacy of biologics that block single cytokines [5]. In fact, our results suggest that agents inhibiting diverse inflammatory pathways (e.g., JAK inhibitors, which have been used with some success in individual PPP cases [33, 34]) might deliver better clinical outcomes than targeted monoclonal antibodies. In this context, a single-cell dissection of the signaling hubs that are deregulated in PPP (e.g., the JAK1/JAK3 or JAK2/TYK2 complex) holds the promises of identifying novel therapeutic targets for this severe and disabling disease.

Acknowledgments

We are grateful to all the patients and volunteers who took part in this study.

The APRICOT and PLUM study team: In addition to A David Burden, Christopher EM Griffiths, Nick J Levell, Richard Parslew, Andrew E Pink, Nick J Reynolds, Richard B Warren, Jonathan N Barker, Catherine H Smith and Francesca Capon, who are authors, the following team members facilitated patient recruitment and data processing for the APRICOT clinical and the PLUM study: David Baudry (Guy's Hospital, London), Victoria Cornelius (Imperial College London), Helen

Lachmann (Royal Free Hospital, London), Helen McAteer (The Psoriasis Association, Northampton), Freya Meynell (Guy's Hospital, London), Prakash Patel (Guy's Hospital, London), Angela Pushparajah (Guy's Hospital, London), Rosemary Wilson (Guy's Hospital, London).

Data availability

The bulk and single-cell RNA-seq data reported in this paper have been uploaded to the publicly accessible Gene Expression Omnibus repository (series accession number GSE185858).

References

1. Burden AD, Kirby B. Psoriasis and related disorders. In: Griffiths CEM, Barker JN, Bleiker T, Chalmers RJ, Creamer D, editors. Rook's Textbook of Dermatology. Chichester: Wiley-Blackwell; 2016.
2. Twelves S, Mostafa A, Dand N, Burri E, Farkas K, Wilson R, et al. Clinical and genetic differences between pustular psoriasis subtypes J Allergy Clin Immunol 2019; 143:1021-6.
3. Benzian-Olsson N, Dand N, Chaloner C, Bata-Csorgo Z, Borroni R, Burden AD, et al. Association of Clinical and Demographic Factors With the Severity of Palmoplantar Pustulosis. JAMA Dermatol 2020.
4. Mossner R, Frambach Y, Wilsmann-Theis D, Lohr S, Jacobi A, Weyergraf A, et al. Palmoplantar Pustular Psoriasis is Associated with Missense Variants in CARD14, but not with loSs-of-Function Mutations in IL36RN in European Patients. J Invest Dermatol 2015:2538-41.
5. Obeid G, Do G, Kirby L, Hughes C, Sbidian E, Le Cleach L. Interventions for chronic palmoplantar pustulosis: abridged Cochrane systematic review and GRADE assessments. Br J Dermatol 2020.
6. Cro S, Cornelius VR, Pink AE, Wilson R, Pushpa-Rajah A, Patel P, et al. Anakinra for palmoplantar pustulosis: results from a randomized, double-blind, multicentre, two staged, adaptive placebo controlled trial (APRICOT). Br J Dermatol 2021.
7. Mrowietz U, Burden AD, Pinter A, Reich K, Schakel K, Baum P, et al. Spesolimab, an Anti-Interleukin-36 Receptor Antibody, in Patients with Palmoplantar Pustulosis: Results of a Phase IIa, Multicenter, Double-Blind, Randomized, Placebo-Controlled Pilot Study. Dermatol Ther (Heidelb) 2021.

8. Mrowietz U, Bachelez H, Burden AD, Rissler M, Sieder C, Orsenigo R, et al. Secukinumab for moderate-to-severe palmoplantar pustular psoriasis: Results of the 2PRECISE study. J Am Acad Dermatol 2019; 80:1344-52.
9. Terui T, Kobayashi S, Okubo Y, Murakami M, Zheng R, Morishima H, et al. Efficacy and Safety of Guselkumab in Japanese Patients With Palmoplantar Pustulosis: A Phase 3 Randomized Clinical Trial. JAMA Dermatol 2019.
10. Navarini AA, Burden AD, Capon F, Mrowietz U, Puig L, Koks S, et al. European Consensus Statement on Phenotypes of Pustular Psoriasis. J Eur Acad Dermatol Venereol 2017:1792-9.
11. Wohnhaas CT, Leparc GG, Fernandez-Albert F, Kind D, Gantner F, Viollet C, et al. DMSO cryopreservation is the method of choice to preserve cells for droplet-based single-cell RNA sequencing. Sci Rep 2019; 9:10699.
12. Zheng GX, Terry JM, Belgrader P, Ryvkin P, Bent ZW, Wilson R, et al. Massively parallel digital transcriptional profiling of single cells. Nat Commun 2017; 8:14049.
13. Schafflick D, Xu CA, Hartlehnert M, Cole M, Schulte-Mecklenbeck A, Lautwein T, et al. Integrated single cell analysis of blood and cerebrospinal fluid leukocytes in multiple sclerosis. Nat Commun 2020; 11:247.
14. Korsunsky I, Millard N, Fan J, Slowikowski K, Zhang F, Wei K, et al. Fast, sensitive and accurate integration of single-cell data with Harmony. Nat Methods 2019; 16:1289-96.
15. Stuart T, Butler A, Hoffman P, Hafemeister C, Papalexi E, Mauck WM, 3rd, et al. Comprehensive Integration of Single-Cell Data. Cell 2019; 177:1888-902 e21.
16. Aran D, Looney AP, Liu L, Wu E, Fong V, Hsu A, et al. Reference-based analysis of lung single-cell sequencing reveals a transitional profibrotic macrophage. Nat Immunol 2019; 20:163-72.
17. Monaco G, Lee B, Xu W, Mustafah S, Hwang YY, Carre C, et al. RNA-Seq Signatures Normalized by mRNA Abundance Allow Absolute Deconvolution of Human Immune Cell Types. Cell Rep 2019; 26:1627-40 e7.
18. Street K, Risso D, Fletcher RB, Das D, Ngai J, Yosef N, et al. Slingshot: cell lineage and pseudotime inference for single-cell transcriptomics. BMC Genomics 2018; 19:477.
19. Tsoi LC, Rodriguez E, Degenhardt F, Baurecht H, Wehkamp U, Volks N, et al. Atopic Dermatitis Is an IL-13-Dominant Disease with Greater Molecular Heterogeneity Compared to Psoriasis. J Invest Dermatol 2019; 139:1480-9.

20. Garcia G, Godot V, Humbert M. New chemokine targets for asthma therapy. Curr Allergy Asthma Rep 2005; 5:155-60.
21. Homey B, Steinhoff M, Ruzicka T, Leung DY. Cytokines and chemokines orchestrate atopic skin inflammation. J Allergy Clin Immunol 2006; 118:178-89.
22. Klicznik MM, Morawski PA, Hollbacher B, Varkhande SR, Motley SJ, Kuri-Cervantes L, et al. Human CD4(+)CD103(+) cutaneous resident memory T cells are found in the circulation of healthy individuals. Sci Immunol 2019; 4.
23. Cano-Gamez E, Soskic B, Roumeliotis TI, So E, Smyth DJ, Baldrighi M, et al. Single-cell transcriptomics identifies an effectorness gradient shaping the response of CD4(+) T cells to cytokines. Nat Commun 2020; 11:1801.
24. Kiner E, Willie E, Vijaykumar B, Chowdhary K, Schmutz H, Chandler J, et al. Gut CD4(+) T cell phenotypes are a continuum molded by microbes, not by TH archetypes. Nat Immunol 2021; 22:216-28.
25. Stockinger B, Omenetti S. The dichotomous nature of T helper 17 cells. Nat Rev Immunol 2017; 17:535-44.
26. Tortola L, Jacobs A, Pohlmeier L, Obermair FJ, Ampenberger F, Bodenmiller B, et al. High-Dimensional T Helper Cell Profiling Reveals a Broad Diversity of Stably Committed Effector States and Uncovers Interlineage Relationships. Immunity 2020; 53:597-613 e6.
27. Wambre E, Bajzik V, DeLong JH, O'Brien K, Nguyen QA, Speake C, et al. A phenotypically and functionally distinct human TH2 cell subpopulation is associated with allergic disorders. Sci Transl Med 2017; 9.
28. Jabeen R, Goswami R, Awe O, Kulkarni A, Nguyen ET, Attenasio A, et al. Th9 cell development requires a BATF-regulated transcriptional network. J Clin Invest 2013; 123:4641-53.
29. Cosmi L, Maggi L, Santarlasci V, Capone M, Cardilicchia E, Frosali F, et al. Identification of a novel subset of human circulating memory CD4(+) T cells that produce both IL-17A and IL-4. J Allergy Clin Immunol 2010; 125:222-30 e1-4.
30. Irvin C, Zafar I, Good J, Rollins D, Christianson C, Gorska MM, et al. Increased frequency of dual-positive TH2/TH17 cells in bronchoalveolar lavage fluid characterizes a population of patients with severe asthma. J Allergy Clin Immunol 2014; 134:1175-86 e7.

31. Cosmi L, Santarlasci V, Maggi L, Liotta F, Annunziato F. Th17 plasticity: pathophysiology and treatment of chronic inflammatory disorders. Curr Opin Pharmacol 2014; 17:12-6.
32. Xu W, Li R, Sun Y. Increased IFN-gamma-producing Th17/Th1 cells and their association with lung function and current smoking status in patients with chronic obstructive pulmonary disease. BMC Pulm Med 2019; 19:137.
33. Koga T, Sato T, Umeda M, Fukui S, Horai Y, Kawashiri SY, et al. Successful treatment of palmoplantar pustulosis with rheumatoid arthritis, with tofacitinib: Impact of this JAK inhibitor on T-cell differentiation. Clin Immunol 2016; 173:147-8.
34. Mossner R, Hoff P, Mohr J, Wilsmann-Theis D. Successful therapy of palmoplantar pustulosis with tofacitinib-Report on three cases. Dermatol Ther 2020; 33:e13753.

Figure Legends

Figure 1. Transcription profiling of PPP non-lesional skin reveals a prominent Th2 gene signature. (**A**) Volcano plot displaying genes that are differentially expressed in non-lesional vs. control skin. Dotted horizontal and vertical lines represent significance (FDR<0.05) and fold-change (log2FC>|0.5|) thresholds, respectively. (**B**) Ten most significantly enriched pathways detected among the genes that are differentially expressed in non-lesional PPP skin. (**C**) Hub and spokes representation of key upstream regulators (IFNG, IL4 and IL13) and their over-expressed target genes. (**D**) Overlap between the genes differentially expressed in non-lesional PPP, atopic dermatitis (AD) and psoriasis (Pso) skin. Statistical significance was calculated with Fisher's exact test. (**E**) Relative mRNA expression of Th1, Th2 and Th17 genes in PPP non-lesional skin. Data are presented as mean +/- SD. As not all biopsies yielded the same amount of mRNA, some samples could not be analyzed for all target genes. *P<0.05 (Mann-Whitney test).

Figure 2. Single-cell RNA sequencing of PBMCs reveals an increased abundance of memory CD4+ T cells in PPP patients. (**A**) UMAP plot showing that the examined cells (n=93,262) form 13 separate clusters. NK: natural killer cells. (**B**) UMAP plot illustrating the expression of key marker genes in the same 93,262 cells. (**C**) Heatmap displaying the expression of marker genes across the 13 cell populations. (**D**) Stacked bar plot showing the abundance of the 13 cell populations within the PBMCs of each donor. (**E**) Increased abundance of memory CD4+ T cell clusters in PPP cases (n=7) compared to healthy controls (HC, n=12). The box plots show medians and inter-quartile ranges, with whiskers illustrating minimum and maximum values. **P <0.01; ***P<0.001 (Mann-Whitney test) (**F**) Plot showing the expression of key T-cell markers in the six CD3+ clusters.

Figure 3. The memory CD4+ T cells of PPP patients are skewed towards a Th17 phenotype. (**A**) Percentage of memory CD4+ T cells annotated as Th1, Th2 or Th17 by SingleR. (**B**) Expression (normalised Unique Molecular Identifier (UMI) counts) of master transcription factors driving Th1 (*TBX21*), Th2 (*GATA3*) and Th17 (*RORC*) differentiation. The box plots show medians and inter-quartile ranges. HC, healthy controls; *P<0.05; **P<0.01; ***P<0.001 (Mann-Whitney test).

Figure 4. Characterization of GATA3+/CD161+ memory CD4+ T cells. **(A)** Heatmap illustrating the expression levels of key marker genes in Th2, Th17 and dual-positive cells, selected on the basis of simultaneous GATA3 and CD161 expression. **(B)** Bubble plot showing minimal expression of HPGDS, PTGS2 and PPARG in dual-positive cells. **(C)** Histogram illustrating the frequency distribution of Th2, Th17 and dual-positive cells during pseudotime. Naïve CD4+ T cells were included in the analysis as a reference undifferentiated population. **(D)** Plots showing the expression of individual marker genes during pseudotime. **(E)** Elevated frequency of dual-positive cells in PPP cases compared to healthy controls (HC). The box plots show median and inter-quartile ranges. $^{**}P<0.01$ (Mann-Whitney test).

Figure 5. Flow cytometry experiments confirm the elevated frequency of GATA3+/CD161+ memory CD4+ T cells among affected individuals. A comparison of PPP cases (n=6) and healthy controls (HC, n=6) shows: **(A)** increased abundance of Th17 (CD161+) cells among the skin-homing (CLA+) memory CD4+ T cells of affected individuals. **(B-C)** increased abundance of CD161+GATA3+ cells among skin-homing (B) and total memory CD4+ T cells (C) of affected individuals. Memory CD4+ T cells were gated as a CD3+/CD4+/CD45RA- lymphocyte population. Skin homing cells were identified as a CLA+ subset. Representative contour plots are shown on the left, with fluorescence minus one (FMO) negative controls for each antibody. The box plots on the right show medians and inter-quartile ranges. $^{*}P<0.05$; $^{**}P<0.01$ (Mann-Whitney test).

Figure 6. Immune fluorescence analysis of non-lesional PPP skin. A representative confocal microscopy image shows GATA3+/CD161+ T-cells (indicated by arrows) infiltrating the upper dermis. Scale bars, 50 µm. The dermal-epidermal junction is highlighted by a dotted line.

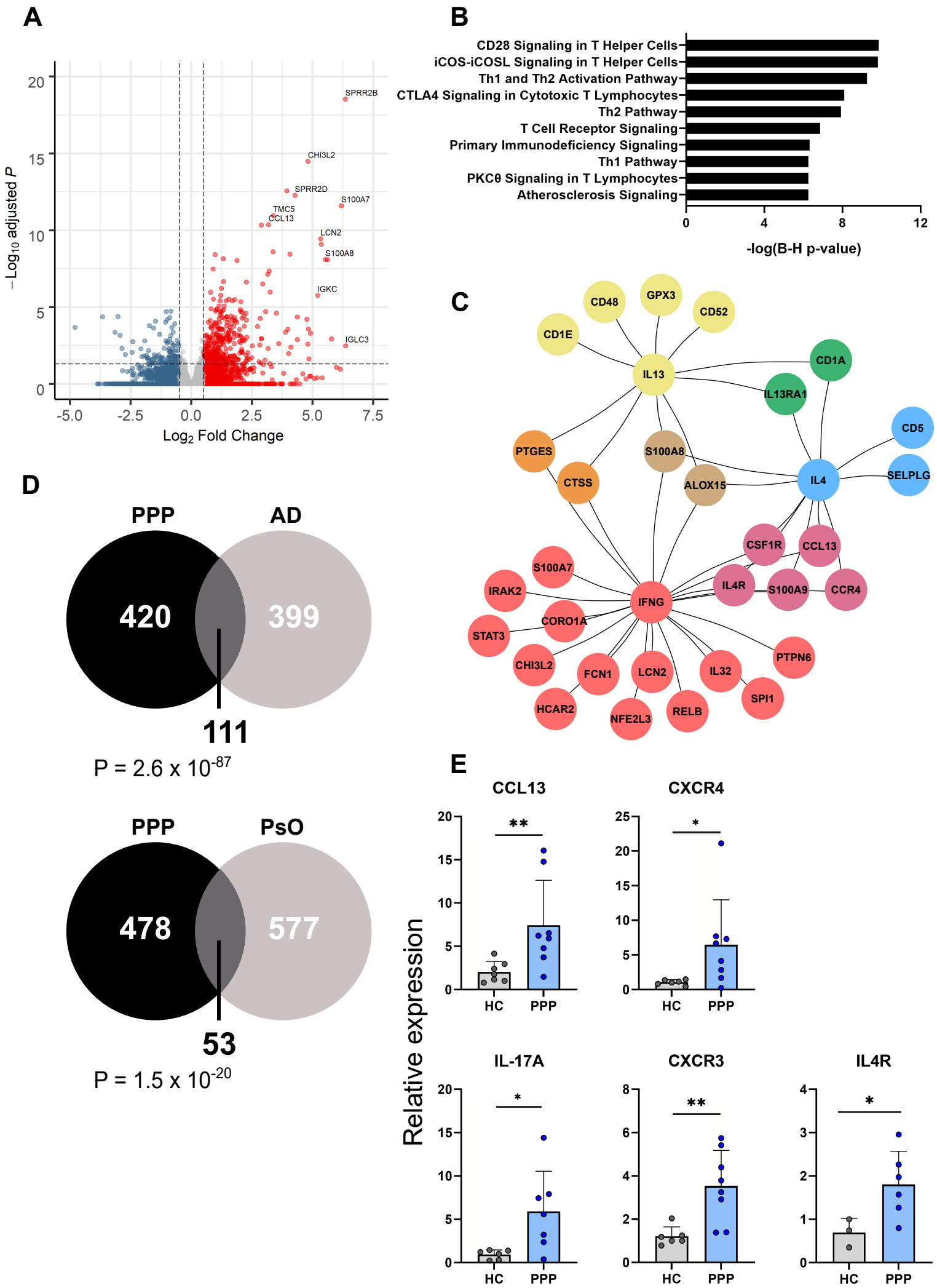
A
SPRR2B
CHI3L2
SPRR2D
S100A7
TMC5
CCL13
LCN2
S100A8
IGKC
IGLC3
−Log10 adjusted P
Log2 Fold Change
B
CD28 Signaling in T Helper Cells
iCOS-iCOSL Signaling in T Helper Cells
Th1 and Th2 Activation Pathway
CTLA4 Signaling in Cytotoxic T Lymphocytes
Th2 Pathway
T Cell Receptor Signaling
Primary Immunodeficiency Signaling
Th1 Pathway
PKCθ Signaling in T Lymphocytes
Atherosclerosis Signaling
-log(B-H p-value)
C
CD48
GPX3
CD52
CD1E
CD1A
IL13
IL13RA1
CD5
PTGES
S100A8
CTSS
ALOX15
IL4
SELPLG
CSF1R
CCL13
S100A7
IL4R
S100A9
CCR4
IRAK2
IFNG
CORO1A
STAT3
PTPN6
CHI3L2
FCN1
LCN2
IL32
SPI1
HCAR2
NFE2L3
RELB
D
PPP
AD
420
399
111
P = 2.6 x 10-87
PPP
PsO
478
577
53
P = 1.5 x 10-20
E
CCL13
CXCR4
IL-17A
CXCR3
IL4R
Relative expression
HC
PPP

Figure No.2

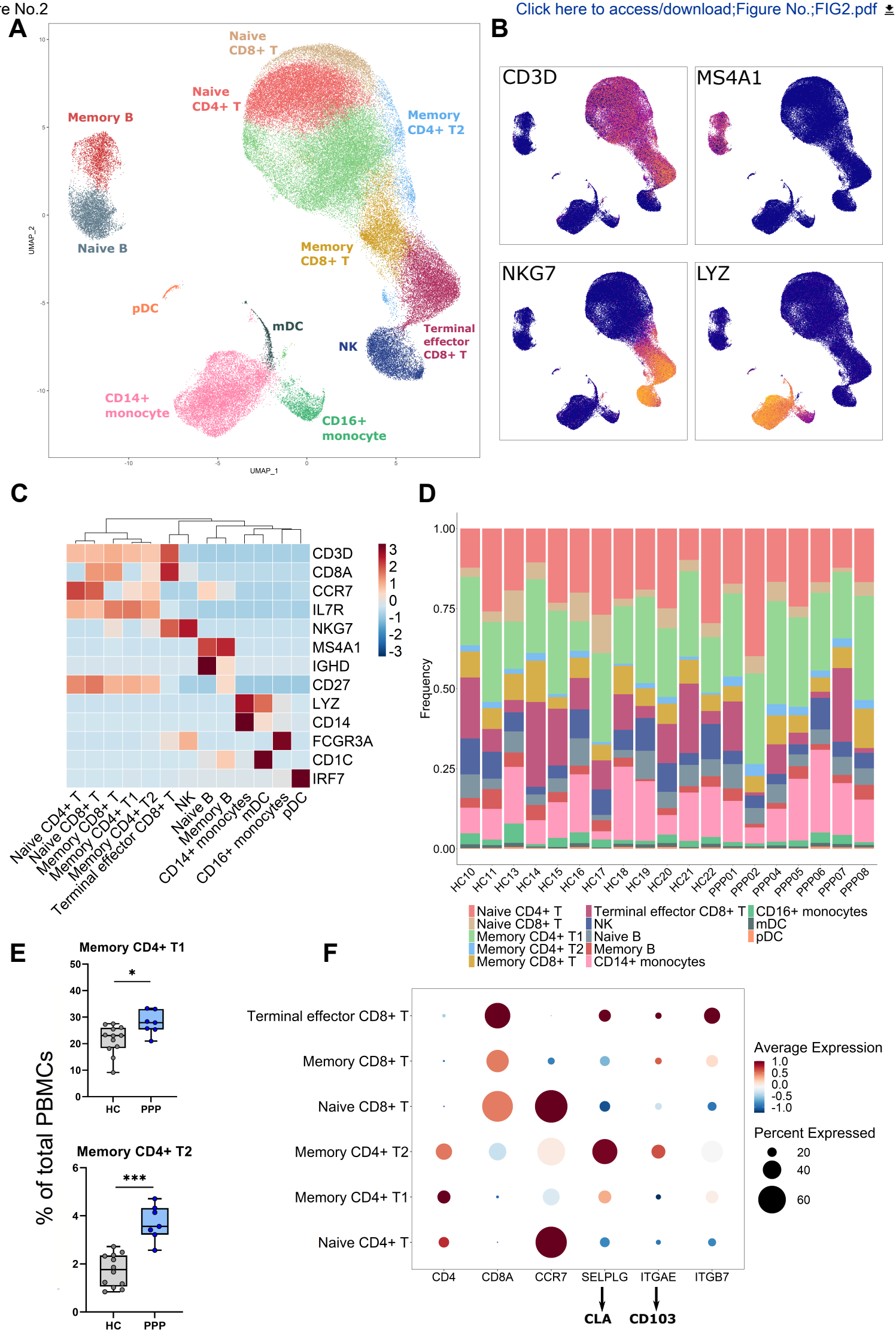

Figure No.3

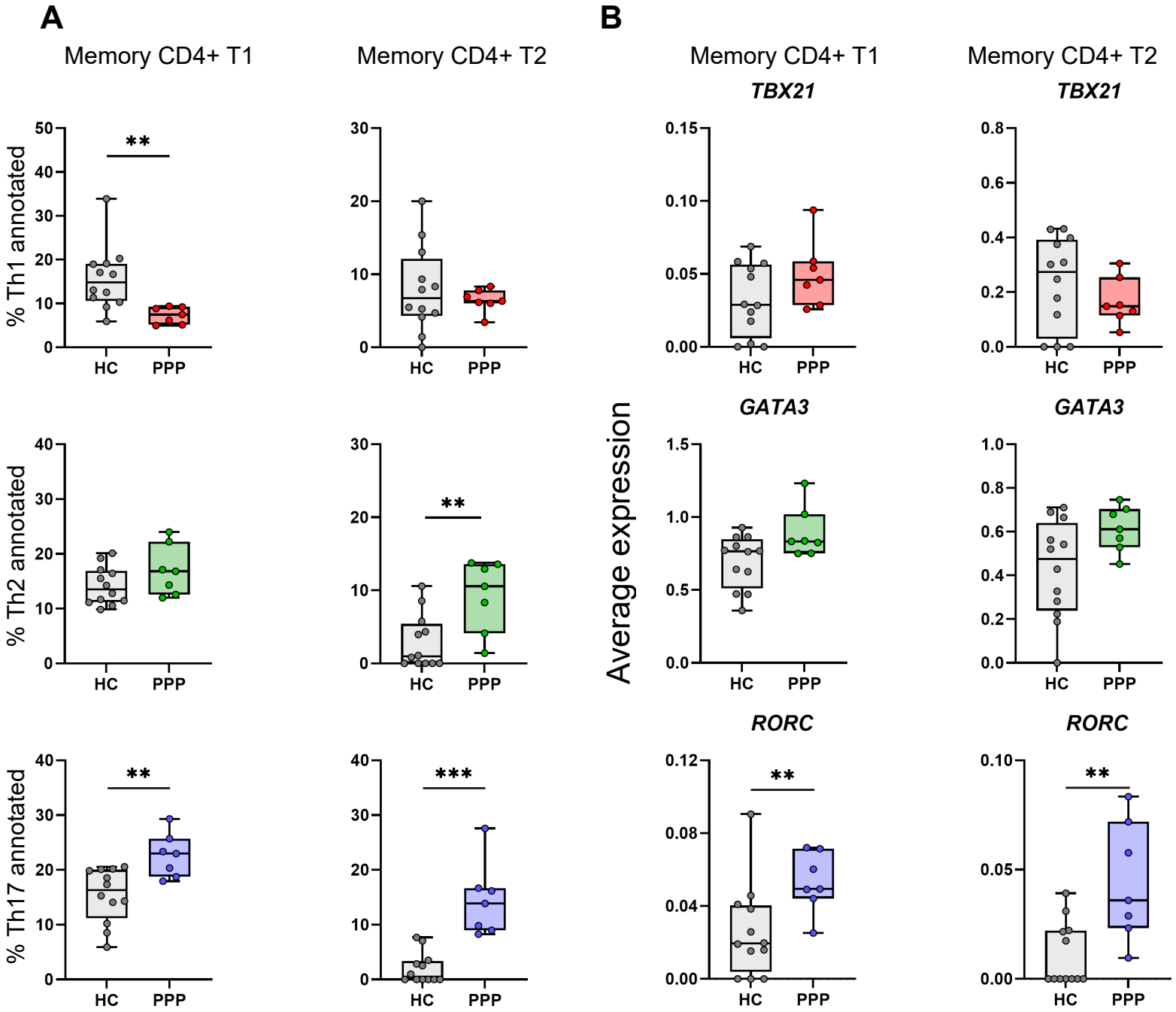

Figure No.4

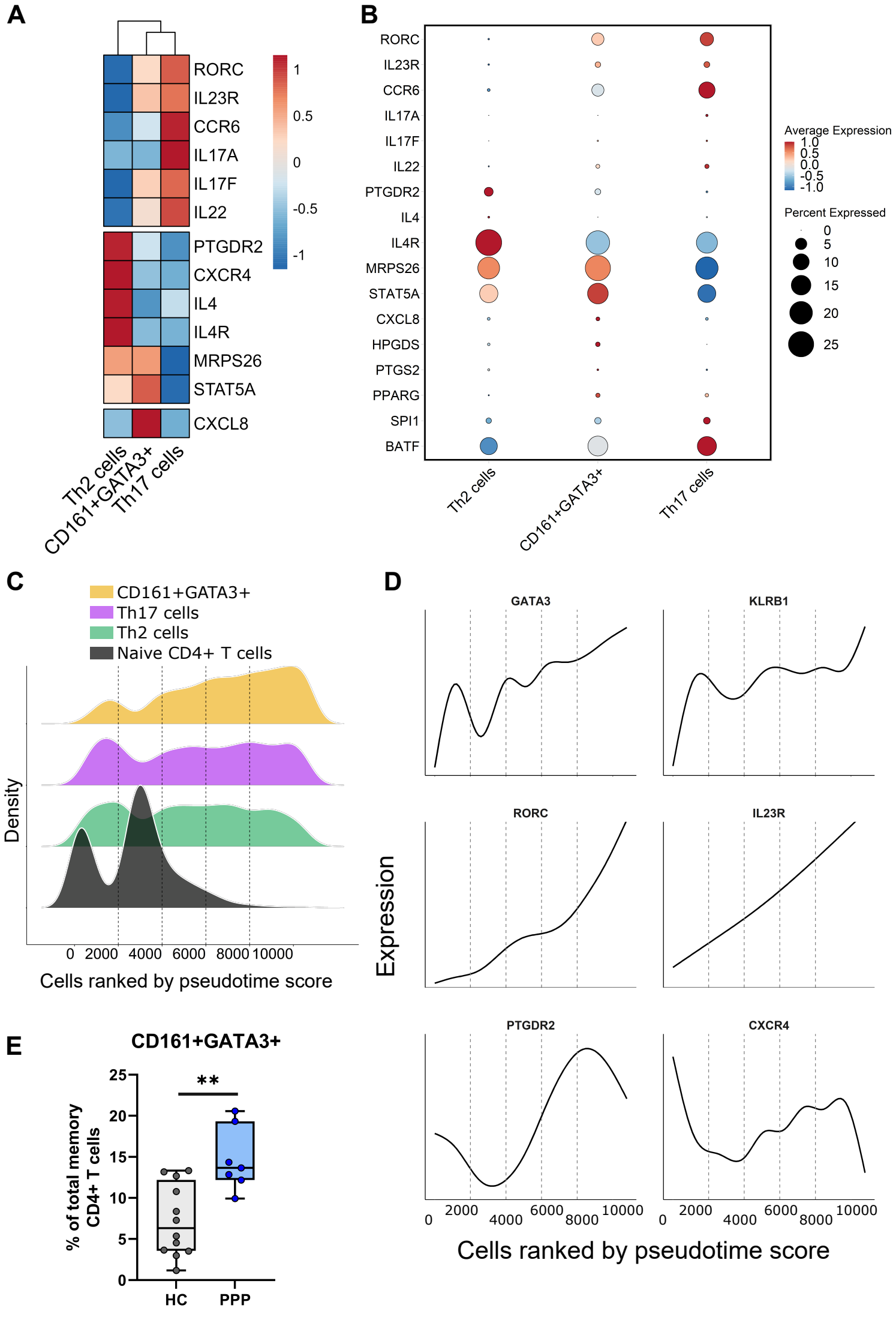

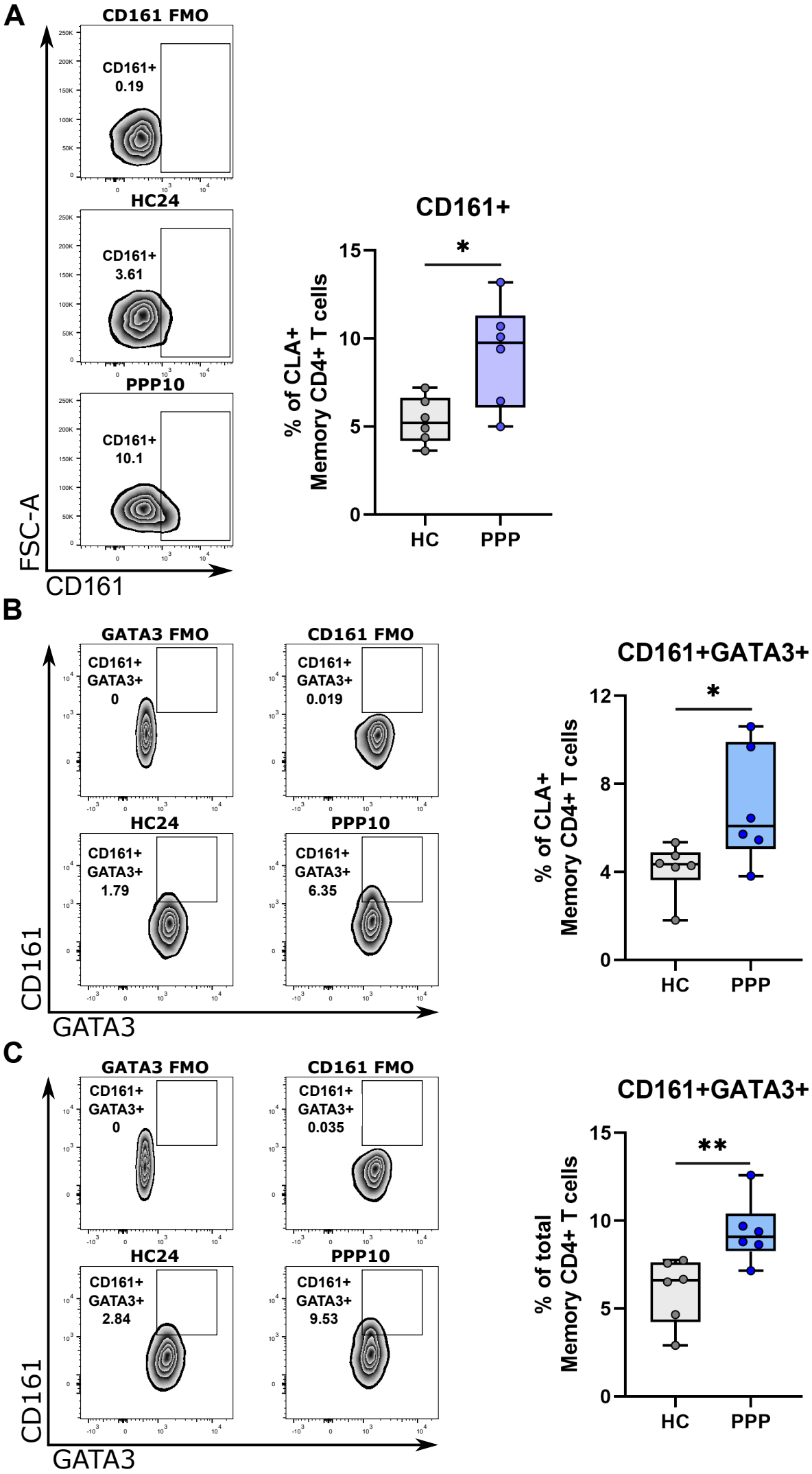

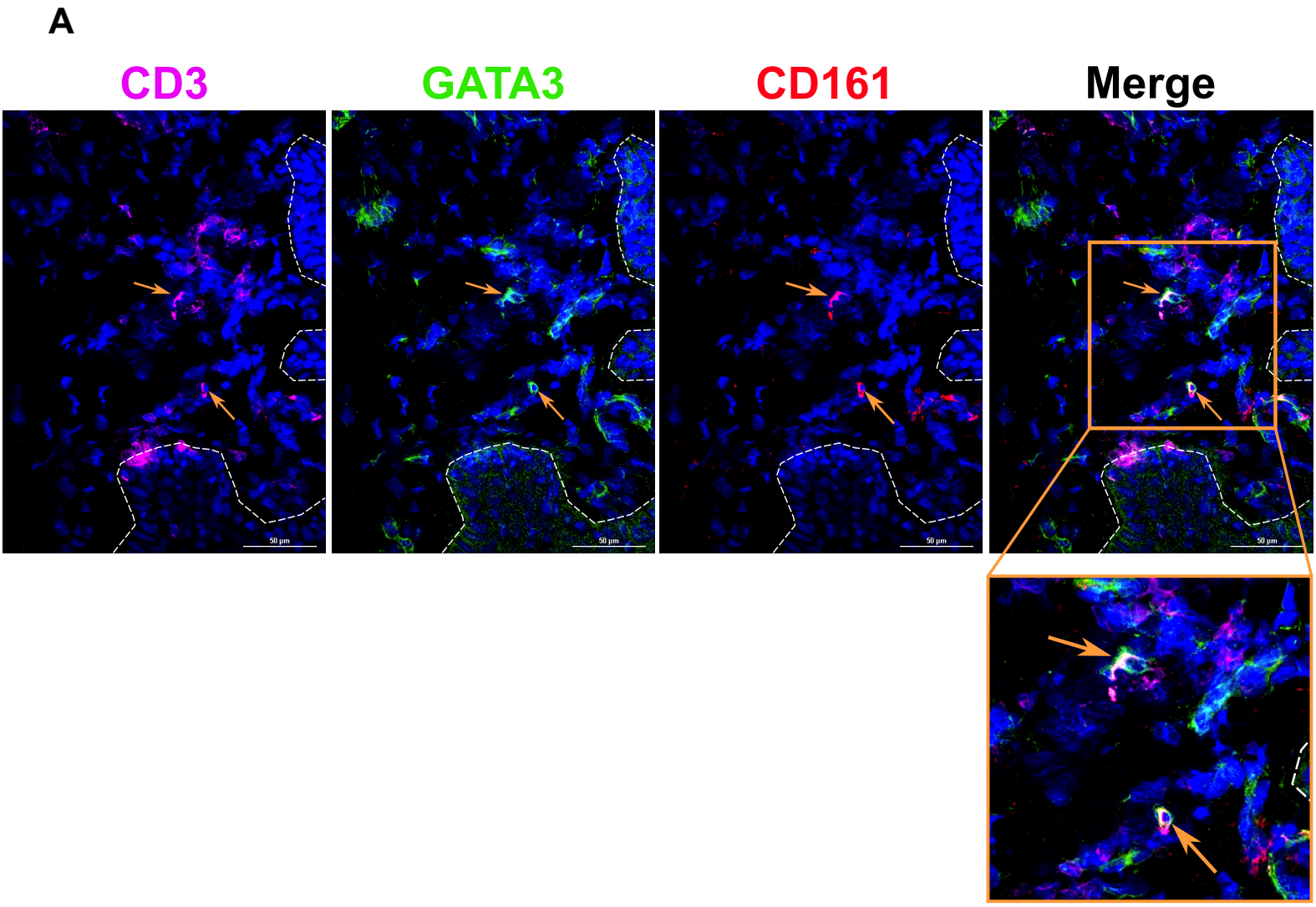

Supplementary Figure No.E1

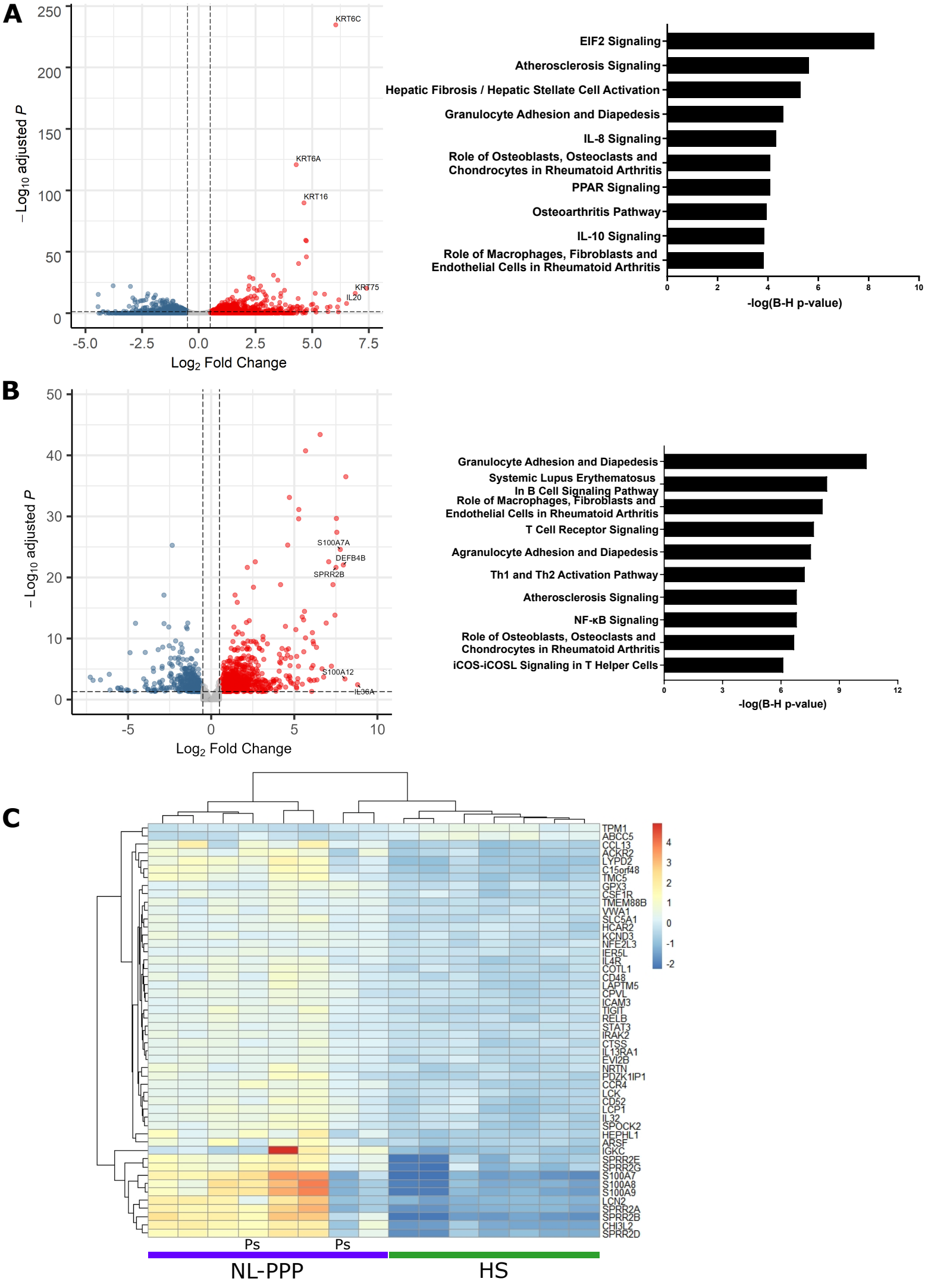

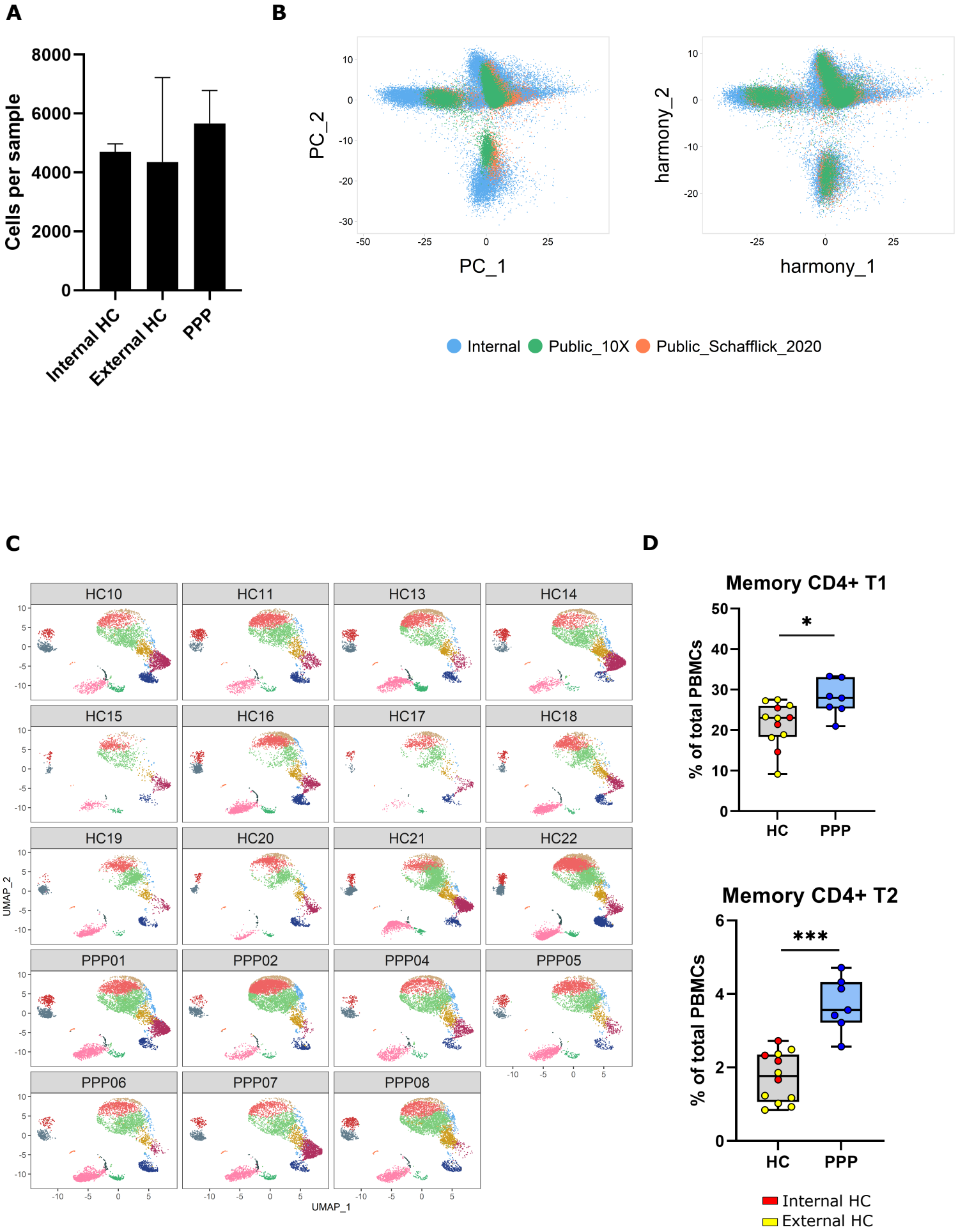
A
Cells per sample
8000
6000
4000
2000
0
Internal HC
External HC
PPP
B
PC_2
PC_1
harmony_2
harmony_1
Internal
Public_10X
Public_Schafflick_2020
C
HC10
HC11
HC13
HC14
HC15
HC16
HC17
HC18
HC19
HC20
HC21
HC22
PPP01
PPP02
PPP04
PPP05
PPP06
PPP07
PPP08
UMAP_2
UMAP_1
D
Memory CD4+ T1
% of total PBMCs
*
HC
PPP
Memory CD4+ T2
% of total PBMCs
***
HC
PPP
Internal HC
External HC

Supplementary Figure No.E3

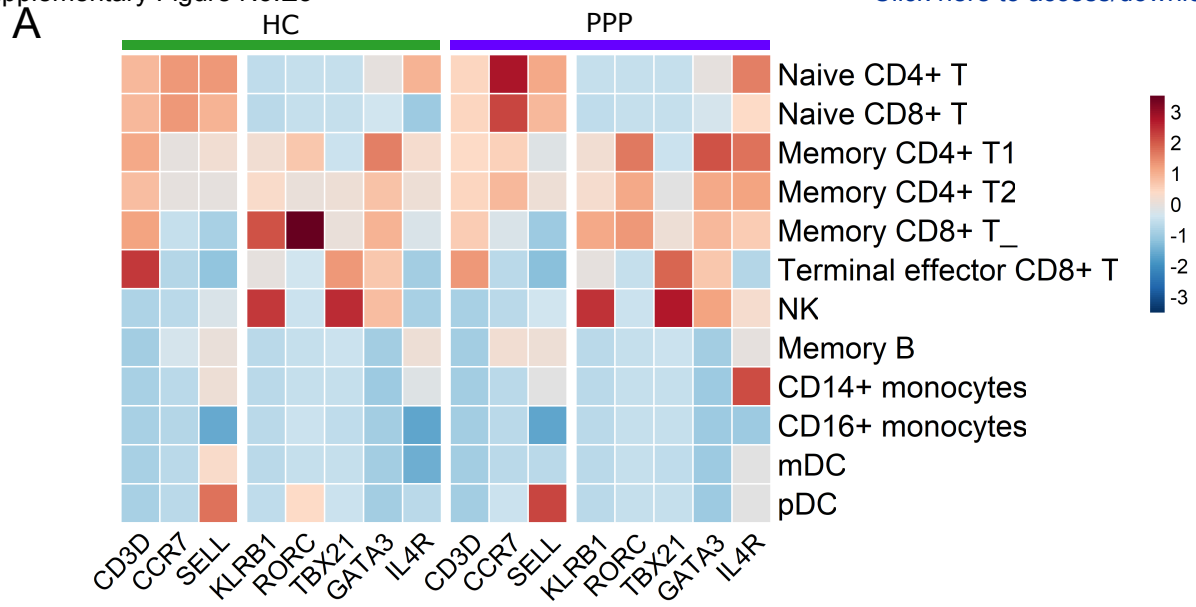

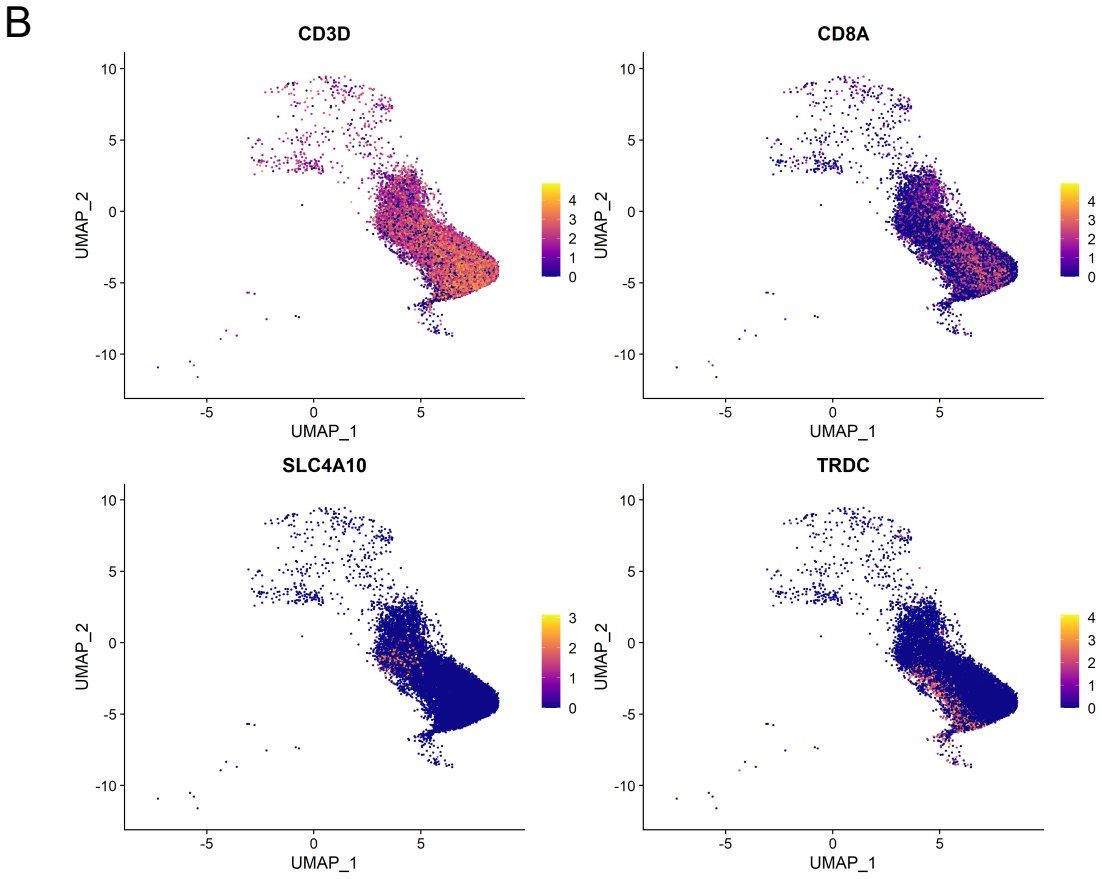

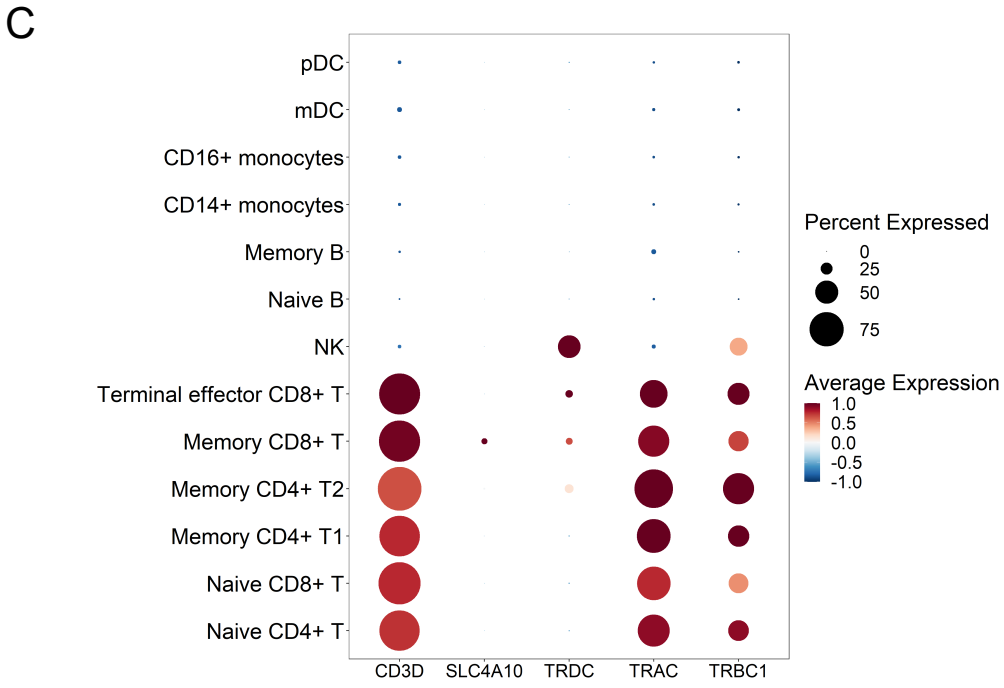

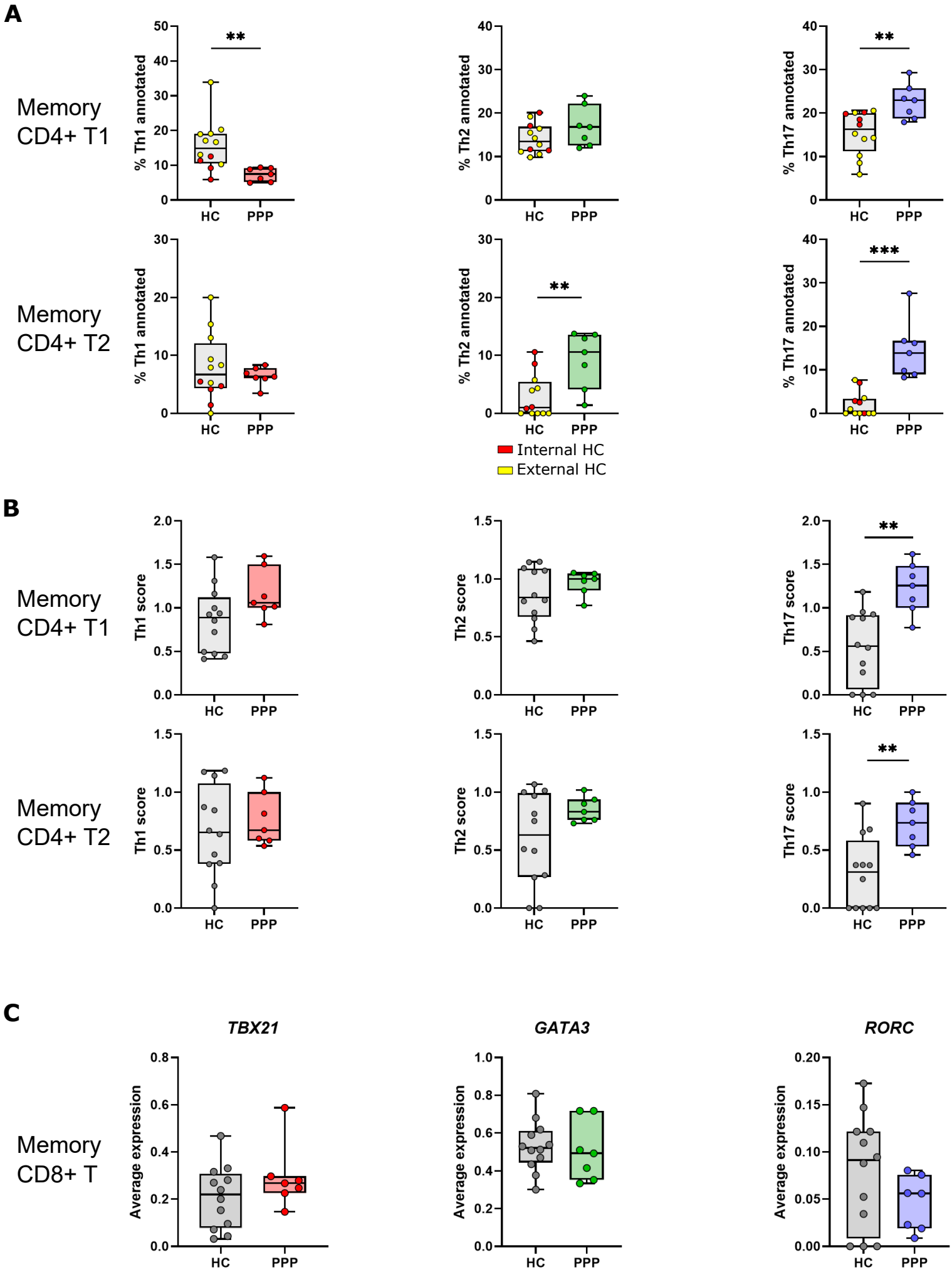
A
Memory CD4+ T1
Memory CD4+ T2
% Th1 annotated
% Th2 annotated
% Th17 annotated
HC
PPP
**
***
Internal HC
External HC
B
Th1 score
Th2 score
Th17 score
C
Memory CD8+ T
TBX21
GATA3
RORC
Average expression

A

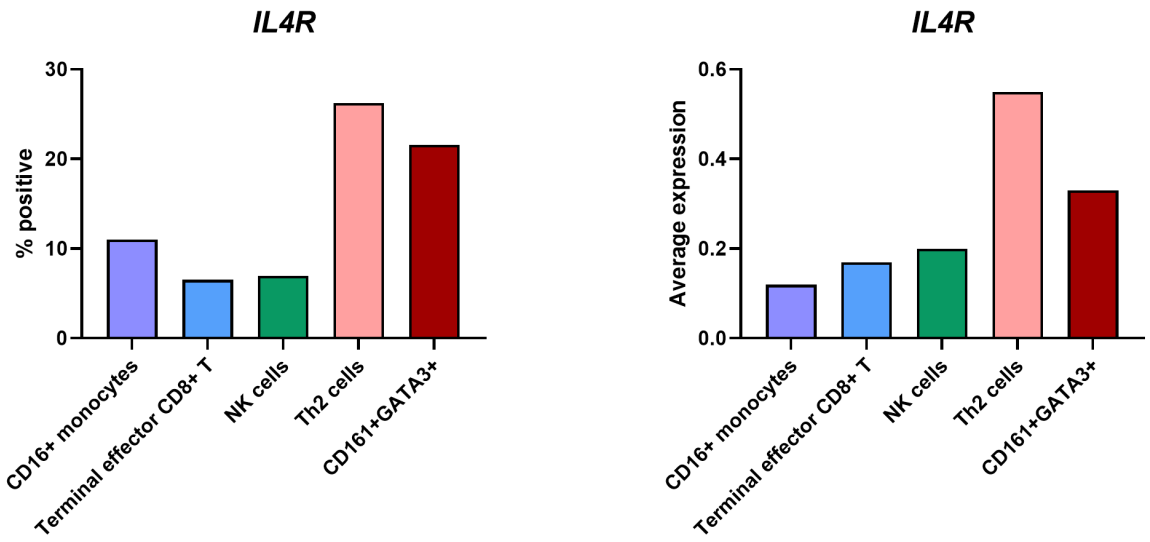
IL4R
% positive
30
20
10
0
CD16+ monocytes
Terminal effector CD8+ T
NK cells
Th2 cells
CD161+GATA3+
IL4R
Average expression
0.6
0.4
0.2
0.0
CD16+ monocytes
Terminal effector CD8+ T
NK cells
Th2 cells
CD161+GATA3+

B

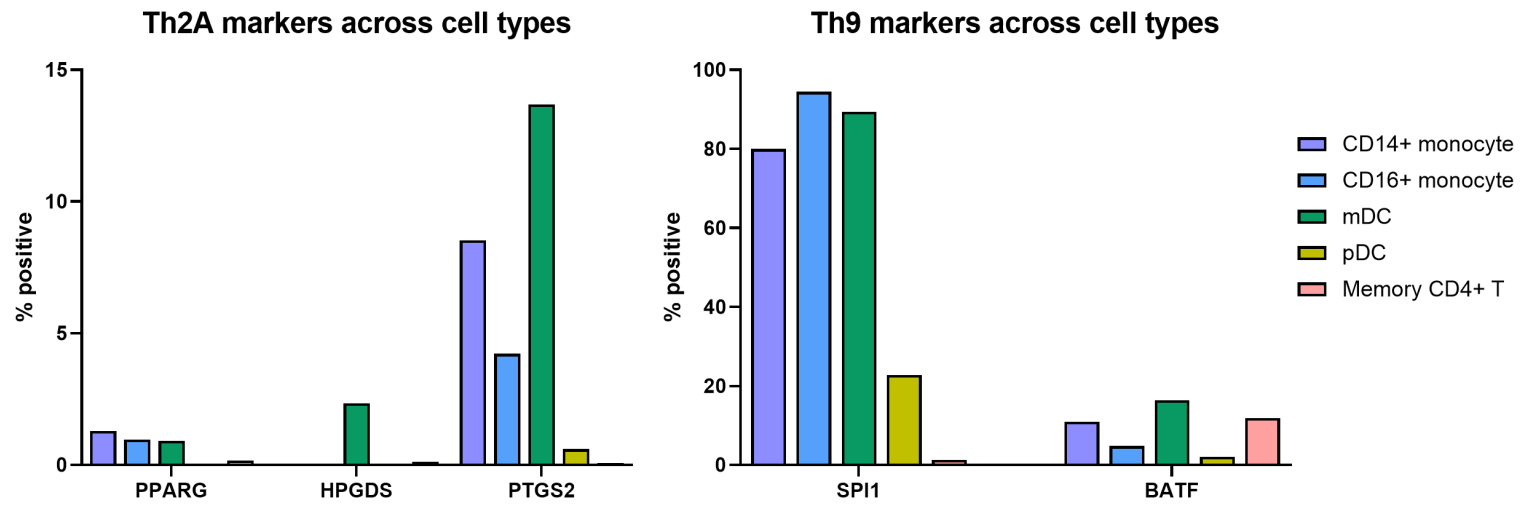
Th2A markers across cell types
% positive
15
10
5
0
PPARG
HPGDS
PTGS2
Th9 markers across cell types
% positive
100
80
60
40
20
0
SPI1
BATF
CD14+ monocyte
CD16+ monocyte
mDC
pDC
Memory CD4+ T

C

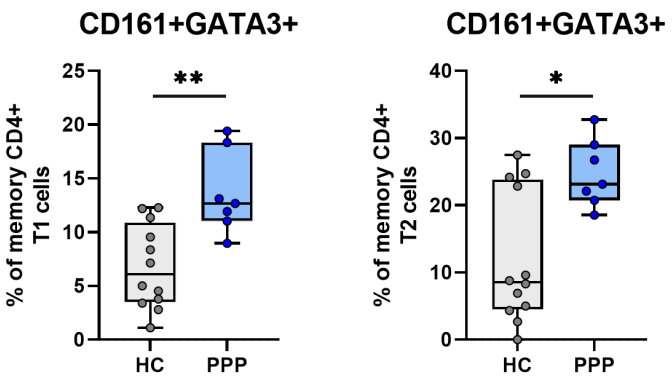
CD161+GATA3+
% of memory CD4+ T1 cells
25
20
15
10
5
0
**
HC
PPP
CD161+GATA3+
% of memory CD4+ T2 cells
40
30
20
10
0
*
HC
PPP

A

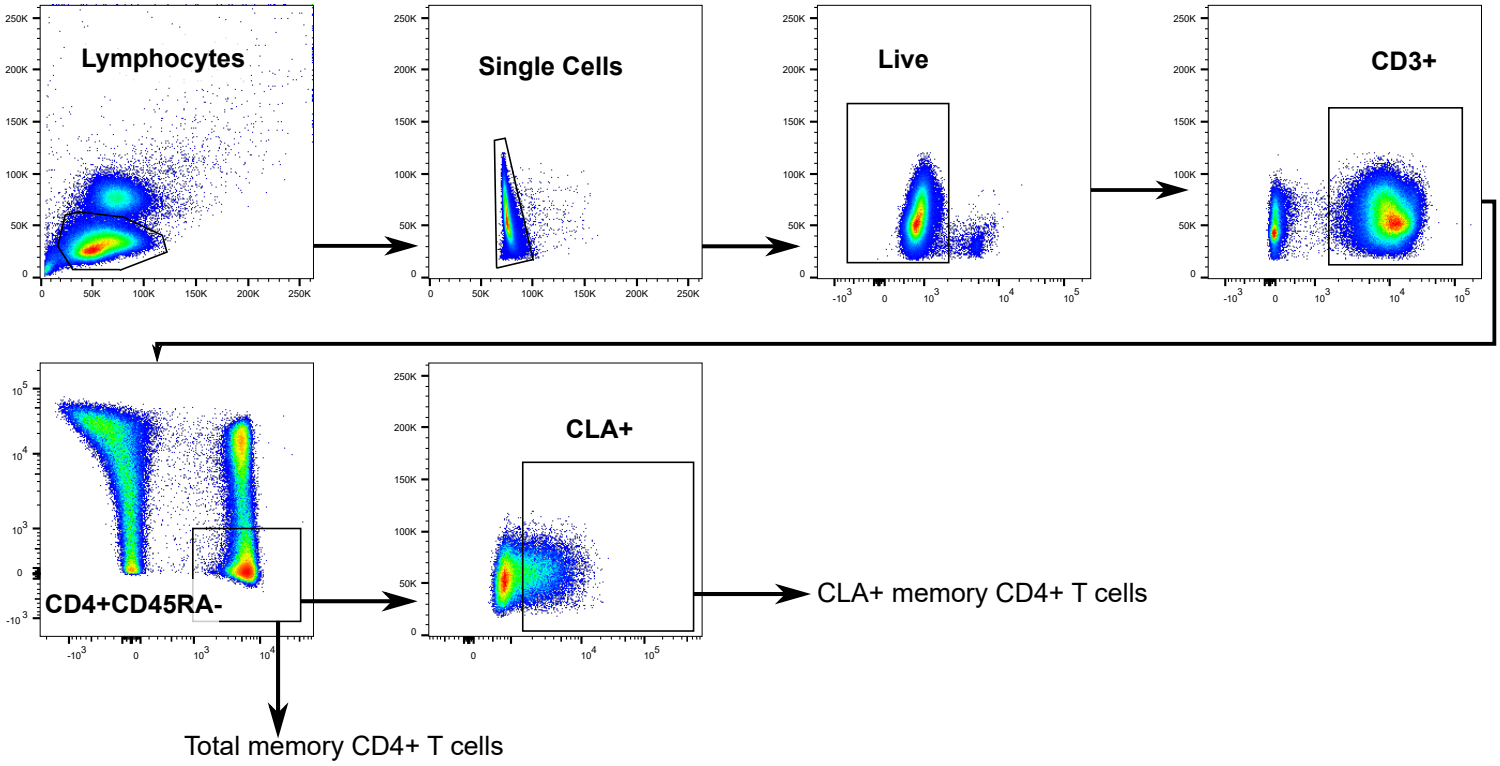

B

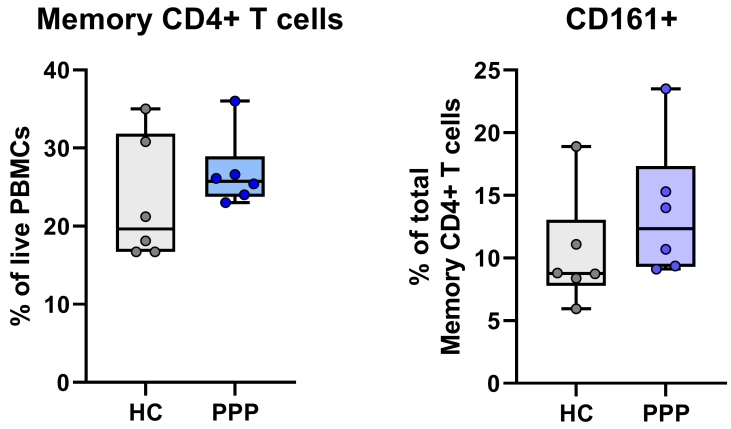

C

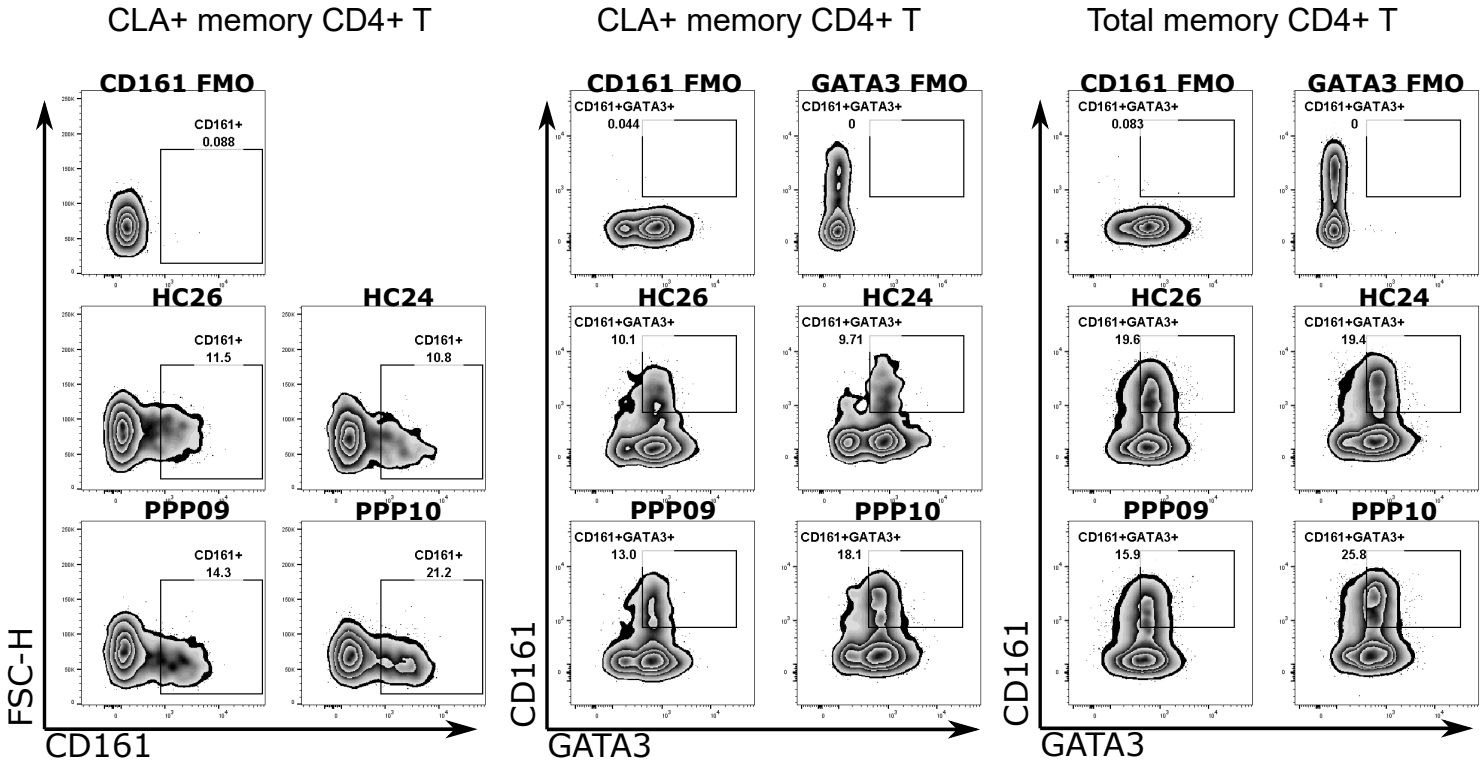

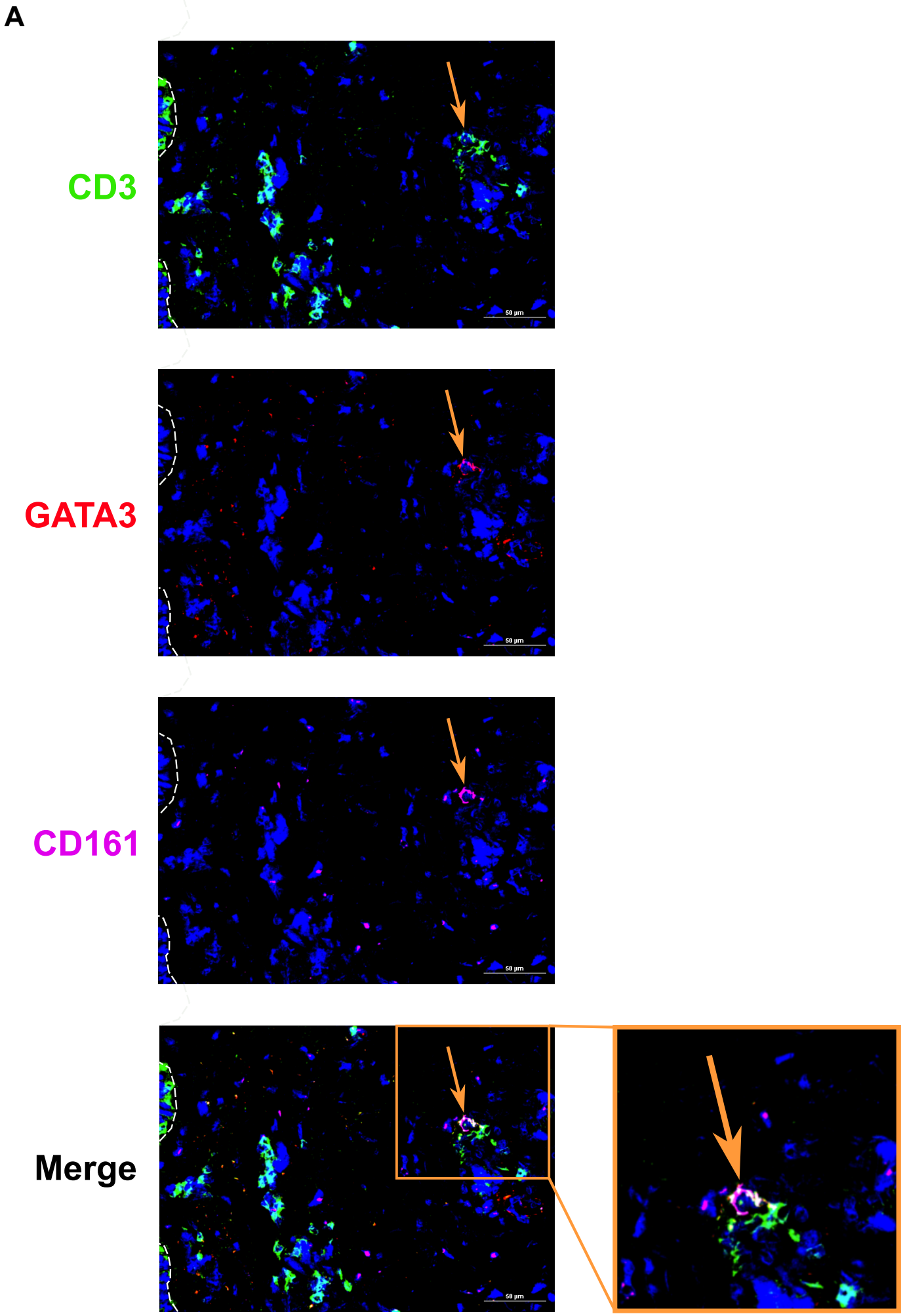
A
CD3
GATA3
CD161
Merge
50 μm
50 μm
50 μm
50 μm

Supplementary Methods

RNA-sequencing data analysis

The quality of the sequence data was assessed using FastQC. Alignment against the GRCh38 human genome was implemented in STAR[1]. Read counts produced by HTseq-count were used as input for the differential expression analysis, which was performed with DESeq2[2] , using sex and biopsy site (palm or sole) as co-variates. For the comparison of lesional vs non-lesional biopsies, information on sample pairs was used as a term in the design formula. Genes were considered upregulated if the log2(fold change) exceeded 0.5 (FDR<0.05). The same computational pipeline was used to process the atopic dermatitis and psoriasis datasets, which were retrieved from the Gene Expression Omnibus (GEO identifier: GSE121212). Differentially expressed genes detected in non-lesional PPP skin were used as input for pathway and upstream regulator enrichment analyses (IPA, Qiagen). IFNγ- IL4- and IL13-centered networks were visualised with the igraph v1.0.1 R Package.

Real-time PCR

Following reverse transcription with the nanoScript2 kit (Primerdesign), real-time PCR was undertaken with a PrecisionPLUS Master Mix with SYBR and ROX (Primerdesign). The following primer pairs were used:

CXCR3: 5'-CCATGGTCCTTGAGGTGAGTG-3'; 5'-AGCTGAAGTTCTCCAGGAGGG-3'

CXCR4: 5'-GAGGGGATCAGTATATACACTTCAG-3'; 5'-ACGGAAACAGGGTTCCTTCAT-3'

CCL13: 5'-ACATGAAAGTCTCTGCAGTGCTTC-3'; 5'-AGTAGATGGGACGTTGAGTGCAT-3'

CCL22: 5'-ATTACGTCCGTTACCGTCTG-3'; 5'-TAGGCTCTTCATTGGCTCAG-3'

IL4R: 5'-AAACGACCCGGCAGATTTCA-3'; 5'-AATCCCAGACTTCAGGGTGC-3'

Transcript levels were normalised to *B2M* expression.

Flow-cytometry

PBMCs were incubated with LIVE/DEAD™ Fixable Near-IR (Invitrogen) dye, Human TruStain FcX™ Fc receptor blocker (Biolegend) and antibodies against the markers of interest. For intracellular staining cells were fixed and permeabilised with the eBioscience™ Foxp3/Transcription Factor Staining Buffer Set, prior to incubation with anti-GATA3. All cells were acquired on a BD Fortessa LSR instrument. Data was analysed using FlowJo v10 software. Antibody details are reported in Table E6 and the gating strategy is illustrated in Figure E5.

33 *Immunofluorescence microscopy*

34 Tissue sections (8µm) cut from a frozen skin biopsy were stained with 1:30 mouse anti-human
35 CD3 (clone UCHT1, eBioscience), 1:30 rat anti-human CD161 (clone W18070C, BioLegend),
36 1:30 rabbit anti-human GATA3 (Biorad). The data were also validated with an alternative set
37 of antibodies: rabbit anti-human CD3 (DAKO), mouse anti-human CD161 (clone B199.2,
38 Biorad), rat anti-human GATA3 (clone TWAJ, Thermofisher). Slides were mounted with
39 Prolong Diamond Antifade Mountant with DAPI (Thermofisher) and imaged using an Eclipse
40 Ti Inverted microscope (Nikon). At least 10 z-stacks images were taken for each sample.

41

42 **Supplementary Figure Legends**

43 **Figure E1**: Transcription profiling of PPP skin. (**A**) Comparison of lesional vs non-lesional skin.
44 Left: volcano plot displaying differentially expressed genes. Dotted horizontal and vertical
45 lines represent significance (FDR<0.05) and fold-change (log2FC>|0.5|) thresholds,
46 respectively. Right: the ten pathways that are most significantly enriched among differentially
47 expressed genes. (**B**) Comparison of lesional vs healthy skin. Left: volcano plot displaying
48 differentially expressed genes. Right: the ten pathways that are most significantly enriched
49 among differentially expressed genes. (**C**) Unsupervised hierarchical clustering of non-lesional
50 PPP (NL-PPP) and healthy skin (HS) samples, based on the analysis of the 50 most differentially
51 expressed genes. The plot demonstrates a clear separation between the two groups, while
52 also showing that individuals with concurrent psoriasis (Ps) do not cluster separately from the
53 rest. This confirms that our analysis was not confounded by the inclusion of these subjects.

54

55 **Figure E2.** Integration of internal and external scRNA-seq samples (**A**) Average number of cells
56 passing quality control among PPP cases, internal and external controls. (**B**) PCA plots showing
57 the cells of internal study participants (PPP cases and internal controls) and external controls,
58 before (left) and after (right) Harmony alignment. (**C**) UMAP plots of individual donors
59 showing that the 13 cell clusters were represented in all samples. (**D**) Frequency of memory
60 CD4+ T cell clusters in healthy controls and PPP cases as in Figure 2E. Here, internal and
61 external controls are highlighted in different colours to show that they are similarly
62 distributed. Of note, the abundance of memory CD4+ T1 cells is higher in cases vs controls
63 (28.0% vs 22.0%), even if external samples are removed. The same applies to the abundance
64 of memory CD4+ T2 cells (3.6% in cases vs 2.2% in controls, once external samples are
65 removed). Box plots show medians and inter-quartile ranges. HC, healthy controls.

66

67 **Figure E3**: Further characterization of T-cell clusters. (**A**) Heatmap confirming the expression
68 of Th1 (*TBX21*), Th2 (*GATA3, IL4R*) and Th17 (*KLRB1, RORC*) markers among memory CD4+ T
69 cells (**B**) The analysis of signature genes for Mucosal-Associated Invariant T-cells (MAIT) and
70 γδ T cells (*SLC4A10*[3] and *TRDC*, respectively) shows that both subsets are present among T
71 lymphocytes (*CD3D* positive cells) expressing *CD8A*. (**C**) Dot plot showing that MAIT cells are
72 found within the memory CD8+ T cluster, while γδ T cells can be detected as *CD3A+/TRDC+*
73 cells in the terminal effector and memory CD8+ T clusters.

Figure E4. Th17 skewing in the memory CD4+ T-cells of affected individuals (**A**) Percentage of memory CD4+ T-cells annotated as Th1, Th2 or Th17, as in Figure 3A. Here, internal and external controls are highlighted in different colours to show that they are similarly distributed. Of note, the frequency of Th17 lymphocytes among memory CD4+ T1 cells is higher in cases vs controls (23.0% vs 19.2%), even if external samples are removed. The same applies to the frequency of Th17 lymphocytes among memory CD4+ T2 cells (13.9% in case vs. 2.7% in controls, once external samples are excluded). (**B**) Th1, Th2 and Th17 transcriptional scores observed in the memory CD4+ T cells of cases and controls. (**C**) Expression (normalised Unique Molecular Identifier (UMI) counts) of master transcription factors driving Tc1 (*TBX21*), Tc2 (*GATA3*) and Tc17 (*RORC*) differentiation. The box plots show medians and inter-quartile ranges. HC, healthy controls. The box plots show median and inter-quartile ranges. HC, healthy controls; **P<0.05;**P<0.01;***P<0.001*.

Figure E5. Additional characterization of GATA3+/CD161+ CD4+ memory T cells. **(A)** Bar plots showing that the percentage of *IL4R*+ cells is similar in Th2 and dual-positive cells, but *IL4R* average expression is weaker in the latter. **(B)** Bar plot showing that Th2A and Th9 markers are readily detectable in our dataset, so that their absence from dual-positive cells cannot be attributed to the low sensitivity of scRNA-seq **(C)** In individuals with PPP, the frequency of dual-positive cells is elevated in both circulating (CD4+ T1 cluster) and skin homing (CD4+ T2) memory CD4+T cells. The box plots show median and inter-quartile ranges. HC, healthy controls; **P<0.05; **P<0.01* (Mann-Whitney test)

Figure E6. (**A**) Flow cytometry gating strategy. The memory CD4+ T cell compartment was defined as a CD3+/CD4+/CD45RA$^-$ lymphocyte population. Skin homing cells were identified as a CLA+ subset (**B**) Frequency of memory CD4+ T cells (left) and Th17 (CD161+) cells (right), in PPP cases (n=6) and healthy controls (HC, n=6). Box plots show medians and inter-quartile ranges. (C) Validation of flow cytometry results with an independent set of antibodies. Staining of four representative samples with alternative anti-CD161 and anti-GATA3 antibodies, confirmed the increased abundance of CD161+ and CD161+/GATA3+ cells among affected individuals.

105 **Figure E7** Immune fluorescence analysis of non-lesional PPP skin using an alternative set of
106 antibodies. A representative confocal microscopy image shows a cell (indicated by an arrow)
107 that simultaneously expresses CD3, GATA3 and CD161. Scale bars, 50 µm. The dermal-
108 epidermal junction is highlighted by a dotted line

Table E1: Participants included in RNA-sequencing studies and follow-up experiments.

	CASES							*CONTROLS*			
Assay (tissue)	*Sample Size*	*Sex*	*Mean Age (+/- SD)*	*Smoking[1] status*	*Mean PPPASI (+/- SD)*	*Comorbidities (n.)*	*Receiving Biologics (n.)*	*Sample size*	*Sex*	*Mean Age (+/- SD)*	*Smoking[1] status*
Bulk RNA-seq (non-lesional skin)	N=8[2]	7F (88%) 1M (12%)	47 (+/- 18)	8 smokers (100%)	15(+/-9)	Psoriasis (2) Hypothyroidism (1) Diabetes (1)	-	N=7	7F (100%)	37 (+/-9)	6 smokers (86%) 1 non-smoker (14%)
Real-time PCR (non-lesional skin)[3]	N=8	8F (100%)	46 (+/- 22)	7 smokers (86%) 1 non-smoker (14%)	17 (+/-11)	Psoriasis (3)	-	N=7	6F (86%) 1M (14%)	39 (+/-10)	6 smokers (86%) 1 non-smoker (14%)
scRNA-seq (PBMCs)	N=7	6F (86%) 1M (14%)	51 (+/-4)	6 smokers (86%) 1 non-smoker (14%)	14 (+/-8)	Diabetes (1) GPP(1); PsA (1)	Secukinumab (1) Guselkumab (2)	N=12	7F (58%) 2M (17%) 3Unk (25%)	37 (+/-9)	5 smokers (42%) 4 non-smokers (33%) 3 unknown (25%)
Flow-cytometry (PBMCs)[4]	N=6	6F (100%)	44 (+/-8)	5 smokers (83%) 1 non-smoker (17%)	13 (+/-7)	Diabetes (1) GPP (1)	Guselkumab (1)	N=6	5F (83%) 1M (17%)	37(+/-4)	2 smokers (33%) 4 non-smokers (66%)

F, Female; GPP, Generalised Pustular Psoriasis; M, Male; PPASI, Palmoplantar pustulosis Area Severity Index; PsA, Psoriatic Arthritis; Unk, unknown;[1]Smokers include both former and current smokers; [2]Three of these individuals also provided lesional biopsies for lesional vs non-lesional skin analysis. In one of these cases, the biopsies were obtained from the sole; [3]Numbers include two cases and three controls who were also analysed in the bulk RNA-seq experiment; [4]including two cases and two controls who were also analysed in the scRNA-seq experiment. All participants were of European descent except one Asian case included in the flow cytometry experiment.

Table E4: scRNA-seq output summary statistics

Sample id (group)	*Estimated n. of cells*	*Total n. of reads*	*Median UMI per cell*	*Mean n. of genes per cell*
PPP01 (case)	7229	339697206	6283	1825
PPP02 (case)	7048	327109350	5888	1548
PPP04 (case)	4742	212341332	6473	1813
PPP05 (case)	4368	198591432	6690	1919
PPP06 (case)	5067	226270351	6561	1829
PPP07 (case)	5192	256403073	6007	1883
PPP08 (case)	5980	291066235	6159	1734
HC10 (control)	4779	204744670	5312	1666
HC11 (control)	4343	192261396	5924	1723
HC13 (control)	4671	217817635	6016	1736
HC14 (control)	4993	226054750	5424	1761

UMI, unique molecular identifier

Table E5: Marker genes used for the annotation of cell clusters

Cell population	*Signature genes*	*Negative markers*[1]
Naïve CD4+ T cells	*CD3D, CCR7,IL7R, CD27, SELL*	*CD8A, S100A4*
Naïve CD8+ T cells	*CD3D, CD8A, CCR7,IL7R, CD27, SELL*	*S100A4*
Memory CD4+ T cells	*CD3D, IL7R, CD27, S100A4*	*CD8A, CCR7, SELL*
Memory CD8+ T cells	*CD3D, CD8A, IL7R, CD27, S100A4*	*CCR7, SELL*
Terminal effector CD8+ T cells	*CD3D, CD8A, NKG7, S100A4*	*IL7R, CCR7*
Natural Killer cells	*NKG7, FCGR3A*	-
Naïve B cells	*MS4A1*/CD20, *IGHD*	-
Memory B cells	*MS4A1*/CD20, *CD27*	*IGHD*
CD14+ monocytes	*LYZ, CD14*	-
CD16+ monocytes	*FCGR3A*	*CD14*
Myeloid dendritic cells	*CD1C, LYZ*	-
Plasmacytoid dendritic cells	*IRF7*	-

[1]Genes whose lack of expression differentiates the population from a closely related subset

Table E6: Flow cytometry antibodies

Target	*Cat number*	*Fluorochrome*	*Supplier*
CD3	300434	BV421	BioLegend
CD4	300518	APC-Cy7	BioLegend
CD45RA	304126	PE-Cy7	BioLegend
CLA	321306	FITC	BioLegend
CXCR3	565223	BUV395	BD
CD161	339912	APC	BioLegend
CD161[1]	130-114-116	APC	Miltenyi-Biotech
GATA3	653804	PE	BioLegend
GATA3[1]	12-9966-41	PE	eBioscience

[1]Antibodies used to generate the validation data presented in Figure E6

Supplemental references

1. Dobin A, Davis CA, Schlesinger F, Drenkow J, Zaleski C, Jha S, et al. STAR: ultrafast universal RNA-seq aligner. Bioinformatics 2013; 29:15-21.
2. Love MI, Huber W, Anders S. Moderated estimation of fold change and dispersion for RNA-seq data with DESeq2. Genome Biol 2014; 15:550.
3. Park D, Kim HG, Kim M, Park T, Ha HH, Lee DH, et al. Differences in the molecular signatures of mucosal-associated invariant T cells and conventional T cells. Sci Rep 2019; 9:7094.